Polyphasic carbonate precipitation in the shallow subsurface: insights from microbially-formed carbonate beds in Upper Miocene sediments of the Tertiary Piedmont Basin (NW Italy).

Polyphasic carbonate precipitation in the shallow subsurface: insights from microbially-formed authigenic carbonate beds in upper Miocene sediments of the Tertiary Piedmont Basin (NW Italy)

M. Natalicchio[a,*], D. Birgel[b], F. Dela Pierre[a,c], L. Martire[a], P. Clari[a], C. Spötl[d], J. Peckmann[b]

[a] *Department of Earth Sciences, University of Torino, 10125 Torino, Italy*

[b] *Department of Geodynamics and Sedimentology, Center for Earth Sciences, University of Vienna, 1090 Vienna, Austria*

[c] *CNR-IGG, 10125 Torino, Italy*

[d] *Institute of Geology and Palaeontology, Leopold-Franzens-University of Innsbruck, 6020 Innsbruck, Austria.*

*Corresponding author:

marcello.natalicchio@unito.it

phone:

+390116705198

Fax:

+390116705339

Eliminato: ¶
¶
¶
¶

ABSTRACT

Authigenic methane-derived carbonates hosted in upper Miocene slope sediments of the Tertiary Piedmont Basin (NW Italy) are studied by a multidisciplinary approach including petrography, stable oxygen and carbon isotopes of carbonates, as well as lipid biomarkers in order to explore the relationship between microbial activity and carbonate precipitation in the shallow subsurface. The studied rocks show a bed parallel geometry and are characterized by dolomitic intergranular cement, which is typified by positive $\delta^{13}C$ values as high as +6.2‰ VPDB. A striking feature of some dolomite beds is an intricate network of septarian-like cracks filled with both injected sediments and polyphasic carbonate cements. Prokaryotic molecular fossils in the dolomite beds comprise archaeol ($\delta^{13}C$: –40‰ VPDB) and various bacterial dialkyl glycerol diethers (DAGEs; $\delta^{13}C$: –30‰ VPDB), strongly suggesting that dolomite precipitation took place at the interface of the zones of archaeal methanogenesis and bacterial sulphate reduction. In contrast, extremely negative $\delta^{13}C$ values of carbonate cements (as low as –56.3‰ VPDB) and various archaeal and bacterial molecular fossils (e.g. pentamethylicosane (PMI): –106‰ VPDB) are recorded in the crack-filling carbonate cements. These cements precipitated due to anaerobic oxidation of methane coupled to sulphate reduction. We propose a scenario for the formation of the diagenetic beds, suggesting that carbonate precipitation was the result of three microbially-driven processes (sulphate reduction, methanogenesis, and, finally, anaerobic oxidation of methane). This unusual sequence was a consequence of a dynamic change of environmental geochemical conditions and fluid circulation patterns that prevailed in the ancient subseafloor during early diagenesis of the unconsolidated sediments. Anaerobic oxidation of methane, which usually predates methanogenesis during increasing burial, postdates methanogenesis in case of the septarian-like beds after the beds were affected by crack formation induced by overcritical pore pressure, allowing the ingress of sulphate-rich water from above and methane-rich water from below.

Keywords:
Authigenic carbonates
Septarian-like cracks

Methanogenesis

Anaerobic oxidation of methane

Stable isotopes

Biomarkers

1. Introduction

Microbially-induced carbonate precipitation occurs within various types of marine sediments, as well as in brackish, and lacustrine sediments. Studies of modern sedimentary environments and culture experiments have shown that the activity of sulphate-reducing bacteria (SRB) can promote the precipitation of carbonate minerals (calcite, aragonite, dolomite) due to an increase in alkalinity related to organic matter degradation (Irwin et al., 1977; Vasconcelos et al., 1995; van Lith et al., 2003; Wright and Oren, 2005; Wacey et al., 2008). Since the metabolism and carbon fixation modes of SRB vary strongly under different environmental conditions (Londry et al., 2004), the resulting fractionation of stable carbon isotopes cannot be easily predicted. Negative $\delta^{13}C$ values of carbonates are often used as evidence for the activity of SRB, but laboratory experiments (Londry et al., 2004) and environmental studies (Heindel et al., 2010) reveal that SRB cannot always be traced by carbonate carbon isotopes.

Below the zone of sulphate reduction, ongoing organic matter degradation is chiefly performed by methanogenic archaea (e.g. Martens and Berner, 1974; Whiticar et al., 1986; Sivan et al., 2007). During methanogenesis, ^{12}C is preferentially incorporated in methane, while the residual pore water becomes enriched in ^{13}C (e.g. Boehme et al., 1996). In these settings, autotrophic methanogenesis is removing CO_2 effectively, which is thought to locally trigger the formation of carbonates by increasing the pH value of pore waters (Budai et al., 2002). These methanogenic carbonates are characterized by positive $\delta^{13}C$ values due to precipitation from a ^{13}C-enriched carbon pool (e.g. Budai et al., 2002). Another scenario leading to dolomite formation assumes the ascent of ^{13}C-enriched fluids from deeper sediment (Meister et al., 2011). In laboratory experiments, Kenward et al. (2009) observed that methanogenesis is indeed capable to

induce dolomite precipitation. Interestingly, ^{13}C-enriched dolomites from the Monterey Formation were found to contain biomarkers of archaea, presumably representing methanogens (Hoffmann-Sell et al., 2011), but an archaeal involvement in dolomite formation is difficult to prove in this case. Similarly as for sulphate-reducing bacteria, it is known for one methanogenic archaeon (*Methanosarcina barkeri*) that a great variability in the extent of carbon isotope fractionations is possible, which is reflected by a wide range of $\delta^{13}C$ values of lipid biomarkers produced by methanogens (Londry et al., 2008).

A further process triggering precipitation of carbonates in sediments is the anaerobic oxidation of methane (AOM; e.g. Ritger et al., 1987; Ussler and Paull, 2008). During its ascent through the sedimentary column, methane is oxidized anaerobically by consortia of archaea and sulphate-reducing bacteria at the base of the sulphate reduction zone (e.g. Hinrichs et al., 1999; Boetius et al., 2000; Orphan et al., 2001, 2002). AOM generates a local increase in alkalinity, thus promoting the precipitation of carbonates. The shape and appearance of subsurface AOM-induced carbonate precipitates are manifold, including carbonate pavements, massive blocks, friable concretions, oil-filled, porous carbonates, and macrofossil-rich carbonates (e.g. Mazzini et al., 2004; Roberts et al., 2010). Generally, authigenic methane-seep carbonates are composed of various calcitic and aragonitic cements (e.g. Roberts and Aharon, 1994; Peckmann and Thiel, 2004; Naehr et al., 2009), and less commonly consist of dolomite (e.g. Peckmann et al., 1999). Most methane-seep carbonates are characterized by extreme ^{13}C-depletions, with $\delta^{13}C$ values as low as –50‰ VPDB or even lower (Peckmann and Thiel, 2004), but some seep limestones do not show low $\delta^{13}C$ values either due to (1) substantial admixture of marine carbonate or (2) superimposed carbonate formation driven by methanogenesis (Kuechler et al., 2011). At some sites, the methane flux can be vigorous enough to reach the sediment surface, enabling aerobic methanotrophic bacteria to flourish (e.g. Niemann et al., 2006; Birgel et al., 2011). In modern environments, AOM and its impact on carbonate precipitation was extensively studied using pore-fluid chemistry, microbiology, lipid biomarkers, element patterns, and stable isotopes (e.g. Hinrichs et al., 1999; Pancost et al., 2000; Knittel et al., 2005; Rossel et al., 2011). However, most of the methods used to unravel microbial processes cannot be applied in ancient sedimentary

sequences. Microbial processes that prevailed during carbonate formation can still be assessed by studying persistent proxies preserved in ancient seep carbonates. Such methods include petrography, stable isotope geochemistry, and lipid biomarkers and their isotopic composition (e.g. Peckmann et al., 1999; Birgel et al., 2008b).

Here we provide a multiproxy data set obtained from authigenic carbonates from upper Miocene deposits of the Tertiary Piedmont Basin. These carbonate rocks belong to a recently identified ancient subsurface seepage system that includes a wide array of carbonate concretions showing different shapes (tubular, cylindrical, ellipsoidal), which formed as a consequence of upward rising methane-rich fluids (Dela Pierre et al., 2010). Among these different types of authigenic methane-derived carbonates, stratiform carbonates are most abundant. In these beds discussed herein not only features typical of methane-seep carbonates are observed, reflecting AOM, but also methanogenesis and sulphate reduction are archived. We particularly focus on the relationship of authigenic carbonate formation and microbial activity as a consequence of the dynamic and changing geochemical conditions and fluid circulation patterns that prevailed in the ancient subseafloor.

2. Geological and stratigraphic setting

The Tertiary Piedmont Basin (TPB) is located in northwestern Italy and is filled with up to 5000 m of upper Eocene to Messinian sediments that unconformably overlie both Alpine metamorphic rocks and Apennine Ligurian Units juxtaposed by the Mesoalpine collision (e.g. Mosca et al., 2009; Fig. 1). The studied area is located in the Borbera-Grue sector in the eastern part of the TPB to the south of the Villalvernia Varzi Line (Fig. 2). The stratigraphic succession of this sector is represented by Oligocene to Pliocene terrigenous sediments deposited unconformably on the Ligurian Unit (Ghibaudo et al., 1985). The upper Miocene part of the succession consists of the Sant'Agata Fossili marls (Tortonian-lower Messinian), the Valle Versa chaotic complex (upper Messinian), and the Cassano Spinola conglomerates (upper Messinian). In the studied sector, (Ripa dello Zolfo area, Fig. 2), the Sant'Agata Fossili marls are further

subdivided into two members (Ghibaudo et al., 1985): (1) the lower member (Tortonian), consisting of outer shelf deposits, which are strongly bioturbated and (2) the upper member (lower Messinian), which hosts the studied carbonate rocks (Fig. 3), deposited on the slope. The grey upper member marls are poorly bedded and show a carbonate content of 15 wt % of the total rock on average (Table 1). They contain abundant fossils (planktic and benthic foraminifera, bivalves, gastropods, and land plant debris), and especially in the uppermost part they are cyclically interbedded with laminated euxinic shales. Like in other parts of the Mediterranean, this cyclic stacking pattern reflects precession-controlled climate changes resulting in the deposition of marls during precession maxima (insolation minima) and laminated shales during precession minima (insolation maxima; e.g. Hilgen at al., 1995). The Sant'Agata Fossili marls are truncated by a regional unconformity (Messinian erosional surface) and are overlain by the chaotic sedimentary bodies of the Valle Versa chaotic complex that consists of blocks of various composition and size floating in a poorly exposed clayey matrix. The blocks include shallow-water evaporites, evaporitic vuggy carbonates, bioclastic carbonates, and authigenic methane-derived carbonates. The overlying Cassano Spinola conglomerates, consisting of upper Messinian deltaic to lagoonal brackish water sediments, correlate with the "Lago Mare" interval recognized all over the Mediterranean area (e.g. Orszag Sperber, 2006).

3. Methods

Field analyses of the lithology and geometry of carbonate-rich beds were carried out in the Ripa dello Zolfo area. Approximately 30 representative samples of the various carbonate beds were selected for petrography and geochemistry studies. The unconsolidated background sediments were sampled for biostratigraphy, palaeoecology, and stable isotope investigations. Semiquantitative analyses on the mineralogical composition of the carbonate fraction focused on the evaluation of the relative abundances of calcite and dolomite, and were carried out on five samples, including both cemented beds and unconsolidated sediments, in an ICP-OES laboratory (Department of Mineralogical and Petrological Sciences, University of Torino), using an IRIS II

Advantage/1000 (Thermo-Jarrel Ash Corporation). Two hundred mg of sample were homogenized and dissolved in 10 ml of acetic acid, in order to remove the carbonates, but preserving the silicates at the same time. The filtered solution was analysed with ICP-OES and the amount of Mg^{2+} and Ca^{2+} was measured. The relative abundance of dolomite in the samples was calculated, assigning the total amount of Mg^{2+}, along with the corresponding amount of Ca^{2+}, to stoichiometric dolomite. The remaining Ca^{2+} was assumed to derive from calcite and was used to calculate the abundance of stoichiometric calcite.

After cutting and polishing carbonate samples, 50 standard petrographic thin sections were prepared. Petrographic and cathodoluminescence observations were carried out by plane-polarized and cross-polarized light microscopy using a CITL 8200 MK3 equipment, operating at about 17 kV and 400 mA. Thin sections were further analysed for their UV-fluorescence with a Nikon microscope with a UV-2A filter block, using ultraviolet light (illumination source 450-490 nm). Scanning electron microscopy (SEM) was carried out on slightly etched polished rock surfaces obtained from the same samples used for thin sections, using a SEM Cambridge Instruments Stereoscan 360 equipped with an energy-dispersive (EDS) microprobe Link System Oxford Instruments.

Microdrilled and micromilled samples were measured for their carbon and oxygen isotope composition. For microdrilled samples, the carbonate fraction was analysed following the method after McCrea (1950) using Finnigan MAT 251 and 252 mass spectrometers. The isotopic ratios are expressed as $\delta^{13}C$ and $\delta^{18}O$ values relative to the VPDB standard (precision < ±0.05‰). These isotope analyses were performed in the *ISO4* Laboratory (Turin, Italy) and in the *MARUM* Stable Isotope Laboratory (Bremen, Germany). Micromilling was conducted at 0.1 mm resolution, using a video-controlled New Wave Research instrument. Sample surfaces were polished before analysis. A trench about 2 mm in width and 0.2 to 0.3 mm in depth was micromilled concordantly to the crystal growth directions. Isotope measurements were performed using a continuous-flow isotope ratio mass spectrometer and an automated carbonate preparation system calibrated against NBS and IAEA standard reference materials. These analyses were performed at the Institute of Geology and Palaeontology of the University of Innsbruck, Austria. The isotopic ratios are expressed as

$\delta^{13}C$ and $\delta^{18}O$ values in per mil versus VPDB. The long-term precision of these analyses is 0.06 and 0.08‰, respectively.

Lipid biomarkers were extracted from two carbonate samples using the preparation procedure described by Birgel et al. (2006b). The samples (ZF 105: 280 g, DM 115: 326 g) were crushed to small pieces for cleaning and decalcification. After decalcification, a cleaning procedure was applied before the samples were subsequently saponified in 6% KOH in methanol. Lipid biomarker extraction was carried out with a microwave extraction system (CEM MARS X) at 80 °C and 600 W with dichloromethane/methanol (3:1) until the solvents used became colourless. The separation of the resulting extracts into four fractions was achieved by column chromatography (500 mg DSC-NH2 cartridges, Supelco) using the indicated amount of solvents: hydrocarbons (4 ml *n*-hexane), ketones (6 ml *n*-hexane/dichloromethane, 3:1), alcohols (7 ml dichloromethane/acetone, 9:1), carboxylic acid fraction (8 ml of 2% formic acid in dichloromethane). Alcohols and carboxylic acids were measured as their trimethyl-silyl (TMS) and methyl ester (ME) derivatives, respectively. All fractions were measured using a gas chromatography–mass spectrometry system (Thermo Electron Corporation Trace MS) equipped with a 30 m R*xi*-5 MS fused silica capillary column (0.32 mm i.d., 0.25 µm film thickness). The carrier gas was He. The gas chromatography (GC) temperature program used was as follows: 60 °C (1 min); from 60 to 150°C at 10°C/min then to 320°C at 4°/min; 27 min isothermal for hydrocarbons or 37.5 min for alcohols and carboxylic acids. Identification of compounds was based on GC retention times and comparison of the obtained mass spectra with published ones. Compound-specific carbon isotope analyses were carried out with a Hewlett Packard 5890 gas chromatograph linked to a Thermo Electron GC-combustion-interface and a Finnigan MAT 252 mass spectrometer. GC conditions were identical to those described above. Carbon isotopes are expressed as $\delta^{13}C$ values relative to the VPDB standard. The carbon isotope measurements were corrected for the addition of TMS- and ME-derivatives. Several pulses of CO_2 with known $\delta^{13}C$ values at the beginning and the end of the runs were used for calibration. Instrument precision was checked using a mixture of *n*-alkanes with known isotopic composition. The analytical standard deviation was <0.6‰. For analysis of stable carbon isotopic compositions of glycerol dibiphytanyl

243 glycerol tetratether (GDGT)-derived biphytanes, tetraethers were subjected to ether-cleavage. An
244 aliquot of non-derivatised alcohols was reacted with HI and acetic acid glacial. The resulting
245 iodides were reduced to hydrocarbons with $LiAlH_4$ in tetrahydrofuran under argon atmosphere. The
246 resulting biphytanes were analysed using GC-FID and GC-MS and subjected to compound-specific
247 carbon isotope analysis as described above.
248
249 **4. Results**
250
251 Nine vertically-stacked carbonate beds have been recognized in the Ripa dello Zolfo area
252 (Fig. 3A). They occur throughout the upper member of the Sant'Agata Fossili marls from the base
253 of this unit up to 5-6 m below the overlying Valle Versa chaotic complex (Dela Pierre et al., 2010).
254 The beds laterally extend for several tens of metres parallel to bedding (Fig. 4). All of them reveal
255 sharp contacts with the enclosing, poorly consolidated marls; locally bed surfaces are wavy. On the
256 basis of different internal features, three types of beds have been recognized: (1) homogeneous
257 beds, (2) septarian-like beds, and (3) brecciated beds (cf. Dela Pierre et al., 2010). Petrographic
258 and isotopic characteristics of these beds have been already described in Dela Pierre et al. (2010).
259 In the following, we will focus only on the septarian-like beds.
260
261 *4.1. Septarian-like beds*
262
263 *4.1.1. Petrography*
264 Three septarian-like beds were found in sections 1 and 2 (Fig. 3A). The most prominent bed,
265 10 to 60 cm in thickness, shows a lateral extension of about 400 m, forming a distinctive marker
266 bed useful for stratigraphic correlation (bed 4 in Figs. 3 and 4). The septarian-like beds reveal the
267 same lithology as the background sediments but are extensively cemented by rhombohedral
268 microcrystals of dolomite (Fig. 5E). Dolomite comprises up to 70 wt.% of the rock (Table 1). An
269 intense fluorescence of the dolomite points to a high content of organic matter (Fig. 5C-D).
270 Sulphide minerals are abundant, chiefly consisting of framboidal pyrite, but many framboids have

been oxidized (Fig. 5F).The most striking feature of the studied beds is an intricate network of several mm- to cm-wide fractures, referred to as septarian-like cracks here because of their similarity to fractures of septarian concretions (cf. Dela Pierre et al., 2010). Fractures are orientated predominantly perpendicular or parallel to bedding (Fig. 5A-B) and many of them are filled either with injected sediments (clastic dykes) or polyphasic carbonate cements (Fig. 5A); in the upper part of the beds, fractures are generally empty (Fig. 5B). The injected sediment consists of mudstone clasts of different size floating within a fine-grained matrix (Dela Pierre et al., 2010). The crack-filling cements consist of isopachous, finely to medium crystalline, fibrous dolomite followed by non-drusy limpid sparry low-Mg calcite interlayered with isopachous turbid fibrous high-Mg calcite. Cathodoluminescence allows to distinguish different cement zones and displays unusual growth geometries, referred to as “pinch-out structures”, which have been interpreted to reflect the past occurrence of gas hydrates within the cracks (cf. Martire et al., 2010). Like in the background sediment, partially oxidized pyrite framboids are abundant both in the injected sediments and in the fracture-filling cements.

One of the septarian beds is locally characterized by further internal complexity (Figs. 3A and 6A). The lower part of this bed was affected by fracturing with fractures oriented at a high angle with respect to the bedding planes, cross-cutting the entire bed from its base to the top. The upper part of the bed is typified by a domal structure, which is approximately 20 cm in height and 40 cm in width. The domal extension of the bed is cemented entirely by dolomite and invaded by a complex network of cm-large empty fractures (Fig. 6A), whereas fractures in the lower part are filled with sediment and carbonate cement (sample DM115; Figs. 3B and 6B). The cement is represented by brownish, fluorescent dolomite crystals that grew directly on the fracture walls. In some fractures different generations of calcite and dolomite spar are arranged to form spherulites up to 3 mm in width (Fig. 6C).

4.1.2 Stable carbon and oxygen isotopes

Several carbonate phases of the septarian-like beds, including the microcrystalline intergranular cement and the fracture-filling cements, have been analysed for their carbon and

oxygen stable isotope signatures. The results of more than 80 analyses are reported in Table 2. In particular for crack-filling cements, the micromill technique was used in order to minimize the errors resulting from the mixing of different carbonate phases. In fact, micromill sampling allowed a separation of cements pertaining to the different diagenetic phases recognized by petrographic and cathodoluminescence analyses. The unconsolidated background sediment, whose carbonate contents reach up to 15 wt.% (see Table 1), was also analyzed for its isotope signature, revealing $\delta^{13}C$ values ranging from –4.1 to –1.1‰ and $\delta^{18}O$ values ranging from –3.0 to –1.5‰ (Fig. 7).

The intergranular dolomite cement mostly yielded positive $\delta^{13}C$ values (as high as +6.2‰, sample ZF106; see Fig. 3B). Interestingly, a sharp trend to lower $\delta^{13}C$ values is observed very close to the cracks of the domal structure (as low as –48‰, samples DM115 and DM142; Fig. 3B). The intergranular cement is characterized by positive $\delta^{18}O$ values (+6 to +7‰). The fracture-filling sediments (clastic dykes) show variable $\delta^{13}C$ values ranging from –32.2 to +3.5‰, $\delta^{18}O$ values vary from +6 to +7‰. Fracture-filling cements were studied in more detail. In the polyphasic cements $\delta^{13}C$ values range from –56.3 to –16.6‰; $\delta^{18}O$ values vary from –6.3 to +6.6‰. Micromill analyses were performed on a 5 mm-wide cement-filled fracture from below the domal structure (Fig. 8; sample DM115), revealing a significant variation of the isotopic composition. The $\delta^{13}C$ values are strongly negative (as low as –56.3‰) with a trend toward higher values in the centre of the fracture (–41‰). The $\delta^{18}O$ values decrease toward the centre, with positive values (as high as +6.6‰) close to the fracture walls and negative values (as low as –6.2‰) in the axial part.

4.1.3 Lipid biomarkers

A molecular fossil (lipid biomarker) approach was applied in order to look into the role of microbial activity in carbonate precipitation (cf. Birgel et al., 2008b). Gas-chromatography amenable molecular fossils were extracted from two different portions of the most prominent septarian-like bed (Fig. 3B). Sample ZF105 derives from the lower portion of this bed; its carbonate component is representative of the intergranular cement. Sample DM115 was taken close to the domal structure and is representative of the fracture-filling cement (Fig. 9).

4.1.3.1. Intergranular cement (sample ZF105). The head-to-tail linked C_{20} isoprenoid phytane was identified in trace amounts in the hydrocarbon fraction. In the alcohol fraction, low amounts of the archaeal diether-bound isoprenoids archaeol and *sn*-2 hydroxyarchaeol were detected (Fig. 9). The content of archaeol is 2-fold higher than that of *sn*-2 hydroxyarchaeol. Both compounds represent membrane lipids of various archaea, including methanogens, halophiles, as well as methanotrophs (e.g. de Rosa and Gambacorta, 1988; Teixidor et al., 1993; Koga et al., 1993, 1998; Hinrichs et al., 1999), whereas phytane can be a degradation product of (1) archaeal membrane lipids (e.g. Birgel et al., 2006b) or (2) chlorophyll (e.g. Goossens et al., 1984). Glycerol dibiphytanyl glycerol tetratethers (GDGTs) were identified as their ether-cleaved biphytanes. GDGTs are sourced by various archaea, for example planktic thaumarchaea and benthic euryarchaea including methanogens and methanotrophs (e.g. DeLong et al., 1998; King et al., 1998; Schouten et al., 2000; Lipp and Hinrichs, 2009). Ether-cleaved biphytanes were not quantified, but a relative distribution of the biphytane chains was determined. The acyclic biphytane is the predominant biphytane with 57% of all biphytanes (Fig. 9), whereas all cyclic biphytanes range between 11 to 16%, with the monocyclic biphytane being least abundant. The $\delta^{13}C$ value found for archaeol is –40‰, that of *sn*-2 hydroxyarchaeol is –43‰, whereas the content of phytane was too low to measure its isotopic composition. Similarly, the overall contents of ether-cleaved biphytanes were too low for isotope analysis, with the exception of acyclic biphytane, which yielded a value of –22‰.

Bacterial compounds are present in the alcohol and carboxylic acid fractions, comprising terminally-branched C_{15} fatty acids (*iso* and *anteiso* fatty acids), with a slight preponderance of the *anteiso* over *iso* fatty acid. Non-isoprenoidal dialkyl glycerol diethers (DAGEs) are dominated by C_{30} DAGEs. Contents of the identified DAGEs are somewhat higher than those of the archaeal isoprenoid diethers archaeol and *sn*-2 hydroxyarchaeol, but lower than those of fatty acids (Fig. 9). Further bacterial molecular fossils are hopanoic acids with 17β(H),21β(H)-32-hopanoic acid being most abundant. The $\delta^{13}C$ values of DAGEs are –30‰ on average. The $\delta^{13}C$ values of bacterial fatty acids could only be measured for the *anteiso*-C_{15} fatty acid (–29‰). The $\delta^{13}C$ values of the 17β(H),21β(H)-32-hopanoic acid was found to be –26‰.

4.1.3.2. Fracture-filling cement (sample DM115). The molecular fossil content of the fracture-filling carbonate cements (sample DM115) differs from that of the intergranular cement. The overall biomarker contents are significantly higher compared to those of the intergranular cement (Fig. 9). The isoprenoid phytane is abundant, the tail-to-tail linked isoprenoid 2,6,10,15,19-pentamethylicosane (PMI) is less abundant. PMI was not observed in sample ZF105. The content of archaeol is slightly higher than in sample ZF105. Interestingly, *sn*-3 hydroxyarchaeol was detected, but not *sn*-2 hydroxyarchaeol. The content of *sn*-3 hydroxyarchaeol was 2.6-fold higher than that of archaeol. Biphytanes were detected after ether-cleavage of GDGTs, but only in minor amounts. However, the distribution of biphytane chains is much different than that of sample ZF105. The content decreases from acyclic, over monocyclic to bicyclic biphytane; tricyclic biphytane is not present. Biphytanic diacids were only identified in this sample. Interestingly, $\delta^{13}C$ values of almost all isoprenoids range from –106‰ (PMI) to –101‰ (*sn*-3 hydroxyarchaeol), with the exception of phytane, which is less ^{13}C-depleted, yielding a value of –70‰.

Compared to the contents of archaeal lipids, the bacterial terminally-branched fatty acids are only present in low amounts, but the mid-chain branched 10Me-C_{16} fatty acid is abundant (Fig. 10). DAGEs were not identified, but two bacterial monoalkyl glycerol monoethers (MAGEs), MAGE-C_{16} and MAGE-10Me-C_{16}, were recognised. 17β(H),21β(H)-hopanoic acids with 31 to 33 carbons were found, with the C_{32} homologue being most abundant. The $\delta^{13}C$ values of all bacterial biomarkers are very similar, ranging from –78 (10Me-C_{16} fatty acid) to –74‰ (hopanoic acids). Only the MAGE-C_{16} is significantly more ^{13}C-depleted (–95‰).

5. Discussion

5.1. Stable isotope and lipid biomarker signatures of the septarian-like beds: evaluating the role of microorganisms in carbonate authigenesis

5.1.1. Intergranular cement

Differently from the narrow range of carbon isotope signals found for the Sant'Agata Fossili marls (–4.1 to –1.1‰), a wide range of $\delta^{13}C$ values (–0.4 to +6.2‰), has been observed for the intergranular dolomite cement of the lower part of the septarian-like beds. The exact formation mechanisms and the possible contribution of microorganisms in diagenetic dolomite formation with positive carbon isotope values is still not well understood, although there is growing evidence that ^{13}C-enriched dolomite indeed forms in the zone of methanogenesis (Mazzullo, 2000; Warren, 2000; Meister et al., 2011). Interestingly, ^{13}C-enriched dolomites of the Miocene Monterey Formation contain abundant molecular fossils of archaea, some of which apparently represented methanogens (Hoffmann-Sell et al., 2011). Carbonates precipitated from an ^{13}C-enriched carbon pool affected by methanogenesis show values as high as +34‰ (Boehme et al., 1996; Greinert et al., 2001; Budai et al., 2002; Meister et al., 2011; Hoffmann-Sell et al., 2011).

A completely different signature characterizes the domal structure of the most prominent septarian-like bed where strongly ^{13}C-depleted intergranular dolomite cement (–48 to –35‰) occurs. This locally confined ^{13}C depletion suggests a causal relationship between the genesis of the fractures in the domal structure and carbonate formation resulting from methane oxidation (cf. Peckmann and Thiel, 2004). This is supported by the strongly negative $\delta^{13}C$ values of the fracture-filling cements (see paragraph 5.1.2.).

Despite this exception, intergranular cement is remarkably enriched in ^{13}C, suggesting that archaeal methanogenesis was a prominent process during the formation of septarian-like beds. Their inventory of molecular fossils confirms that archaea strongly imprinted the early diagenetic environment. The archaeal lipids archaeol and *sn*-2 hydroxyarchaeol occur in many archaeal groups, including various methanogens (e.g. Koga et al., 1998). Their $\delta^{13}C$ values of –40 and –43‰, respectively, do not provide undisputable evidence to constrain the metabolism of the source organisms. These values alone do not allow to judge with certainty if the archaea were methanotrophs, methanogens, or heterotrophic sedimentary archaea, although the latter group appears to synthesize archaeal diethers only in minor amounts (Lipp and Hinrichs, 2009). Other archaeal biomarkers found in the intergranular cement of the septarian-like bed, as for example GDGTs, measured as ether-cleaved biphytanes in this study, help to identify the affiliation of the

411 source organisms and point in another direction than the diethers. The relatively higher content of
412 monocyclic biphytane, as well as a lower relative abundance of the tricyclic biphytane in the
413 intergranular cement compared to fracture-filling cement typifies heterotrophic archaea thriving in
414 the deep biosphere (cf. Biddle et al., 2006; Lipp and Hinrichs, 2009). The observed pattern of
415 archaeal lipids renders unlikely a major contribution of planktic thaumarchaea. Interestingly, an
416 increased relative abundance of acyclic biphytane is also typical for methanogenic archaea
417 (Pancost et al., 2008). A derivation of biphytanes from methanotrophic archaea, on the other hand,
418 is very unlikely, since biphytane patterns of methanotrophic archaea are different (Birgel et al.,
419 2008a). Moreover, other biomarkers of methanotrophic archaea such as PMI and crocetane
420 (Peckmann and Thiel, 2004) were not detected in the intergranular cement. Biomarkers of
421 sulphate-reducing bacteria (SRB), the syntrophic partners of methanotrophic archaea in AOM, are
422 present (*iso* and *anteiso* fatty acids, DAGEs), but their relatively high $\delta^{13}C$ values do not reflect the
423 incorporation of methane-derived carbon, revealing that the source organisms were not involved in
424 AOM. For example, $\delta^{13}C$ values of DAGEs and *anteiso*-C_{15} fatty acid are approximately 10‰
425 higher than those of archaeol and *sn*-2 hydroxyarchaeol.
426 Based on their isotopic composition, biphytanes (acyclic biphytane: –22‰) and archaeal
427 diethers (average –41‰) are apparently not derived from the same source organisms, although
428 the reasoning above suggests that both groups of compounds derive from sedimentary archaea.
429 Heterotrophic sedimentary archaea typically produce lipids with intermediate $\delta^{13}C$ values (Biddle et
430 al., 2006), whereas the isotopic composition of lipids of methanogenic archaea can vary
431 significantly in culture and the environment depending on substrates and conditions (Londry et al.,
432 2008; Hoffmann-Sell et al., 2011). The observed biphytane distributions resemble those of
433 heterotrophic archaea (cf. Biddle et al., 2006), whereas archaeol and *sn*-2 hydroxyarchaeol most
434 likely reflect archaeal methanogenesis. Overall, the biomarker pattern and isotopic signatures of
435 lipids in the ^{13}C-enriched intergranular cements point to dolomite precipitation close to the interface
436 of the zones of methanogenesis (archaeal diethers) and sulphate reduction (terminally-branched
437 fatty acids, bacterial diethers).
438

439 *5.1.2. Fracture-filling cements*

440 In contrast to the intergranular cement, the cement filling cracks shows more negative $\delta^{13}C$
441 values (–56 to –25‰). Such values typify modern (e.g. Aloisi et al., 2000; Ussler and Paull, 2008;
442 Bahr et al., 2010) and ancient seep carbonates (e.g. Peckmann et al., 1999; Campbell et al., 2006;
443 Himmler et al., 2008; Clari et al., 2009). Therefore, these values reflect incorporation of methane-
444 derived carbon, pointing to AOM (e.g. Ritger et al., 1987). However, the less negative values may
445 also point to other sources or a mixture of various sources. Possible carbon sources of the
446 fracture-filling cement include (1) thermogenic methane (cf. Whiticar, 1999), deriving from the
447 Mesozoic sequence underlying the Cenozoic succession, (2) contributions of fluids enriched in
448 heavier hydrocarbons, such as ethane, propane or crude oil (cf. Roberts and Aharon, 1994), (3) a
449 contribution from a carbonate pool affected by methanogenesis, (4) organic matter degradation
450 (Moozley and Burn, 1993; Raiswell et al, 2002), or (5) the contribution of marine dissolved
451 inorganic carbon and skeletal material of marine organisms.

452 The former occurrence of AOM is confirmed by the lipid biomarker data that resemble those
453 of ancient seep carbonates. One of the most abundant and persistent AOM biomarkers is PMI (e.g.
454 Elvert et al., 1999; Peckmann and Thiel, 2004), showing a $\delta^{13}C$ value of –106‰ in the fracture-
455 filling cement. It is accompanied by ^{13}C-depleted archaeol (–102‰) and abundant biphytanic
456 diacids (–105‰) containing 0, 1, and 2 cyclopentane rings. The latter compounds have been
457 described from ancient seep carbonates and have been suggested to represent particularly reliable
458 AOM biomarkers, often revealing the lowest $\delta^{13}C$ values among all AOM-lipids (Birgel et al.,
459 2008a). The *sn*-3 hydroxyarchaeol (–101‰) detected in the fracture-filling cement has been
460 recognized at some seeps, but this compound is rather uncommon and it is unknown by which
461 type of methanotrophic archaea it is produced (Pancost et al., 2001b; De Boever et al., 2009).

462 A further difference from the intergranular cement is the presence of ^{13}C-depleted
463 biomarkers of SRB. However, biomarkers of SRB (10Me-$C_{16:0}$ fatty acid: –78‰; *anteiso*-$C_{15:0}$ fatty
464 acid: –75‰) show very low contents compared to archaeal biomarkers. *Anteiso*-$C_{15:0}$ fatty acid is a
465 biomarker of SRB involved in AOM of rather high specificity (Elvert et al., 2003; Birgel et al.,
466 2006b). 10Me-$C_{16:0}$ is a well known biomarker of SRB, but this compound does not typically occur

467 in SRB involved in AOM. The two non-isoprenoidal MAGEs detected belong to a group of
468 compounds known to be synthesized by mesophilic SRB (Rütters et al., 2001) and have been
469 identified at modern seeps, revealing extreme ^{13}C-depletions (e.g. Hinrichs et al., 2000; Pancost et
470 al. 2001a). In ancient methane-seep limestones, MAGEs were never identified before, suggesting
471 an exceptional preservation of molecular fossils in the fracture-filling cement. The observed
472 hopanoic acids, exhibiting very similar isotopic composition like the other SRB-derived compounds,
473 probably derive from SRB as well, since no molecular fossils of aerobic methanotrophic bacteria
474 were identified such as 3-methylated hopanoids or lanostanes (cf. Birgel and Peckmann, 2008). In
475 summary, the low $\delta^{13}C_{carbonate}$ values as well as molecular fossils and their isotopic compositions
476 reveal that AOM occurred in the fractures of the septarian-like bed and confirm that carbonate
477 precipitation resulted from AOM.
478
479 *5.2. Gas hydrates in the shallow subsurface: insights from oxygen isotopes*
480
481 Apart from carbon isotopes, oxygen isotopes are commonly used to characterize the
482 composition and temperature of pore fluids at the time of carbonate precipitation (e.g. Fritz and
483 Smith, 1970; Vasconcelos et al., 2005). The oxygen isotope composition of carbonates precipitated
484 in equilibrium with early Messinian seawater averages around –2.0‰ for calcite and +2.0‰ for
485 dolomite (e.g. Pierre et al., 1998; Pierre and Rouchy, 2004). The $\delta^{18}O$ values of the studied
486 carbonates show a wide range of both extremely positive values (as high as +7.7‰) as well as
487 negative values (as low as to –6.3‰). The excellent preservation of molecular fossils rules out
488 substantial late diagenetic alteration. The oxygen isotope pattern consequently suggests that the
489 Ripa dello Zolfo authigenic carbonates precipitated from fluids with $\delta^{18}O$ values different from those
490 of normal marine Messinian seawater. Processes that can produce ^{18}O-enrichment include
491 evaporation of sea water (e.g. McKenzie et al., 1979), dehydration of smectite clay minerals
492 (Dählmann and de Lange, 2003), and gas hydrate destabilization (e.g. Aloisi et al., 2000; Pierre
493 and Rouchy, 2004). With respect to the positive $\delta^{18}O$ values of the Ripa dello Zolfo carbonates,
494 Dela Pierre et al. (2010) concluded that the coincidence of positive $\delta^{18}O$ values with negative $\delta^{13}C$

values agrees best with gas hydrate destabilization. This interpretation is further supported by the occurrence of unusual cements within the septarian-like fractures, characterized by pinch-out structures, which have been interpreted as cements resulting from gas hydrate decomposition (Martire et al., 2010).

Negative $\delta^{18}O$ values were not observed in the Ripa dello Zolfo carbonates before (Dela Pierre et al., 2010; Martire et al., 2010). Such values are only found in the fracture-filling cement (Fig. 9) and, in particular, within the last carbonate phase sealing the fractures. These values consequently recorded the isotopic composition of the latest fluids circulating in the cracks. The explanations most commonly brought forward for anomalously low oxygen values are (1) dilution of parent fluids by meteoric waters (Mozley and Burns, 1993), (2) low-temperature alteration of volcanic material (Gieskes and Lawrence, 1981), (3) upward migration of high-temperature fluids (Sample and Kopf, 1995), and (4) formation of gas hydrates (e.g. Pierre and Rouchy, 2004). The absence of volcanoclastic layers in the stratigraphic succession allow to exclude the alteration of volcanic glass. The negative oxygen isotope signatures of the Ripa dello Zolfo carbonates coupled with strongly negative $\delta^{13}C$ values ($\delta^{13}C < -50‰$), also make meteoric fluids an unlikely explanation. Moreover, the severely ^{13}C-depleted carbonates, more consistent with biogenic methane produced in the shallow subsurface than with thermogenic gas, allow to exclude hot, deeply sourced fluids. Finally, structures believed to be related to the former presence of gas hydrates in the sediments suggests that the observed negative $\delta^{18}O$ values in the fracture fillings indeed reflect gas hydrate formation, with the low values resulting from the incorporation of ^{18}O-enriched water in the gas hydrates structure (cf. Ussler and Paull, 1995).

5.3. Genesis of the carbonate-rich beds

A new scenario for the formation of stratiform concretions is proposed here that is based on petrographic and geochemical results, but also builds on data and interpretations of previous studies (Dela Pierre et al., 2010; Martire et al., 2010). The proposed scenario considers the contrasting isotope values and biomarker patterns recognized in the septarian-like beds,

suggesting that different types of microorganisms thrived under varying environmental conditions. The high carbonate content of 47 to 95 wt.% of the studied beds compared to the host marls (<15%) reveals that bed formation occurred during an early diagenetic stage within still soft and porous Messinian muds at shallow depths. The lack of sediment compaction and the absence of chemosymbiotic macrofossils, which are commonly associated with methane seeps at the seafloor, point to a formation in the shallow subsurface. Unlike typical sub-spherical or ellipsoidal concretions, whose formation occurs around a nucleus (e.g. Sellés-Martìnez, 1996; Raiswell and Fisher, 2000), or cylindrical concretions where carbonate precipitation follows the pathway of fluid flow through the sedimentary column (e.g. Clari et al., 2004; De Boever et al., 2009; Nyman et al. 2010), the bedding-parallel geometry of the studied examples points to formation at a geochemical interface parallel to the seafloor (cf. Meister et al., 2008; Dela Pierre et al., 2010).

Three main stages, each of them characterized by different environmental conditions, are purported to explain the genesis of the Ripa dello Zolfo beds (Fig. 10).

5.3.1. Microbial sulphate reduction close to the sediment-water interface

Studies on modern marine sediments demonstrated that bacterial sulphate reduction, i.e. the most common process degrading organic matter apart from aerobic degradation in the marine subsurface, is capable of inducing carbonate precipitation (e.g. Mozley and Burns, 1993). In all Ripa dello Zolfo cemented beds the former occurrence of sulphate reduction is documented by abundant pyrite framboids (Fig. 5F). Moreover, abundant and well-preserved biomarkers of SRB suggest that these bacteria favoured carbonate precipitation (Fig. 10A). However, although sulphate-reduction is usually a dominant biogeochemical process in marine sediments, the lack of moderately low $\delta^{13}C$ values (Fig. 7) typifying this process suggests that only a small amount of carbonate was produced by sulphate reduction in this case. Accordingly, Raiswell and Fisher (2000, 2004) suggested that carbonate precipitation via sulphate reduction is commonly not significant enough to produce extensive cementation in concretions, calling for other processes to contribute to the formation of concretions and diagenetic beds.

551 *5.3.2. Methanogenesis*

552 Initial carbonate precipitation driven by sulphate reduction reduced the sediment pore
553 space, causing a slight reduction of permeability (Fig. 10A). Ongoing sedimentation led to
554 progressive burial and to a relative downward movement of the semi-lithified beds, which were now
555 placed in the zone of archaeal methanogenesis. Here, the residual organic matter not degraded by
556 sulphate-reducing bacteria was decomposed by archaea, as recorded by ^{13}C-enriched dolomite
557 microcrystals (values as high as +6‰; Fig. 10B). *In situ* methanogenesis is further supported by
558 the prominent occurrence of archaeal molecular fossils in the Ripa dello Zolfo beds. These
559 molecules have $\delta^{13}C$ values as low as –43‰, falling between the values typically found for
560 methanogenic and methanotrophic archaea. However, the range of $\Delta_{substrate\text{-}archaeol}$ in methanogens
561 is extremely large (Londry et al., 2008). In laboratory experiments, Londry et al. (2008) found
562 $\Delta_{substrate\text{-}archaeol}$ in autotrophic methanogenic archaea varying from 11 to 43‰, depending on the
563 experimental conditions. In dolomites from the Monterey Formation, a $\Delta_{substrate\text{-}archaeol}$ of 33‰ (n = 4)
564 was reconstructed and interpreted as a signature of methanogenic archaea. In the sample of
565 intergranular cement, the $\Delta_{substrate\text{-}archaeol}$ would have been 46‰, if one uses the mean of the
566 $\delta^{13}C_{dolomite}$ values to assess the stable carbon isotopic composition of CO_2 consumed by
567 methanogens. This fractionation is even larger than the largest fractionation found in the laboratory
568 experiments of Londry et al. (2008). However, based on the $\delta^{13}C_{dolomite}$ values and since the
569 biomarker inventory of the intergranular cement is more typical of methanogenic rather than
570 methanotrophic archaea and very different from the inventory typifying methanotrophic archaea in
571 the fracture-filling cement, it is most likely that methanogenesis was a prominent process.

572

573 *5.3.3. Anaerobic oxidation of methane in newly generated cracks*

574 The continuing cementation of the Ripa dello Zolfo beds generated a permeability barrier
575 that hampered the rise of fluids, which presumably increased the pore pressure. High pore
576 pressure probably induced the opening of septarian-like fractures within those portions of the beds
577 not yet affected by complete cementation (Fig. 10C). Similarly, an increase in pore fluid pressure
578 favoured by long-lasting seepage activity has been considered as a possible mechanism for crack

579 formation and the injection of mud in laterally extensive seep deposits (Peckmann et al., 2011).
580 The sediment injection, the unusual lobed shape of the domal structure, and the associated
581 fracture system placed at high angle to the bedding plane suggest that fluid overpressure, probably
582 related to supply of methane-rich fluid from deeper stratigraphic levels, is responsible for the
583 opening of a set of septarian-like cracks subsequently infilled by sediment. Similar mechanisms
584 have already been inferred for septarian concretions (e.g. Hounslow, 1997; Astin and Scotchman,
585 1988; Pratt, 2001; Scotchman et al., 2002; Bojanowski, 2007). The Ripa dello Zolfo domal
586 structure resembles a cavernous carbonate crusts from the Black Sea, also suggested to reflect
587 deformation of sediments in the very shallow subsurface induced by overpressure (Mazzini et al.,
588 2008). However, shrinkage processes induced by syneresis, and enhanced by the decay of
589 extracellular polymeric substances can also be responsible for the opening of these fractures (cf.
590 Hendry et al., 2006; Dela Pierre et al., 2010).
591 The $\delta^{13}C$ values and biomarker patterns of dolomite and calcite cement filling the septarian
592 cracks confirm that AOM was the dominant biogeochemical process in these cavities. At this stage,
593 the sulphate-methane transition zone was shifted to greater sediment depths. This shift probably
594 resulted from the fracturing itself, which allowed a downward flux of sulphate-rich fluids into the
595 newly formed cracks. With methane coming from below, now penetrating the Ripa dello Zolfo bed
596 after fracturing, AOM proceeded and induced cement formation. The intergranular cements
597 surrounding the cracks of the domal structure, marked by negative $\delta^{13}C$ values, also reflect AOM
598 (Fig.10C), revealing that the matrix of the carbonate bed was still permeable enough to be affected
599 by diagenetic processes. On the basis of the pinch-out geometry of some cements and oxygen
600 isotope values of the crack-filling cements, it has been suggested that methane-rich fluids resulted
601 from gas hydrate decomposition during this stage (Dela Pierre et al., 2010; Martire et al., 2010).
602

603 **6. Conclusions**

604

605 The petrographical, stable isotope, and biomarker data reveal that the upper Miocene Ripa
606 dello Zolfo beds are the product of different biogeochemical processes that induced carbonate

precipitation in the shallow subsurface. The most intriguing feature of the septarian-like beds is the concomitant presence of a wide array of stable isotope compositions typifying different generations of carbonate cements. Strongly variable carbon isotope signatures ($\delta^{13}C$: –56 to +6‰) and molecular fossils reveal that sulphate reduction, methanogenesis, and finally anaerobic oxidation of methane occurred within the same sediment volume and resulted in the formation of the Ripa dello Zolfo septarian-like beds. Whereas first sulphate reduction and then methanogenesis occurred in the pore space of sediments, anaerobic oxidation of methane occurred only later within cracks after the beds had been fractured by overcritical pore pressures. Pore fluid overpressure is further supported by the occurrence of abundant sediment injections, suggesting that opening of cracks and injection of liquefied mud were triggered by seepage activity. This study represents an interesting example for the impact of biogeochemical processes on organic-rich sedimentary strata. It reveals that the sequence of biogeochemical processes – which is governed by the energy yield of the respective processes – can be modified by synsedimentary events. In this case, fracturing of semi-lithified beds allowed anaerobic oxidation of methane to occur after methanogenesis, which is usually the terminal process in the remineralisation of organic matter.

Acknowledgements

Special thanks are due to Catalin Petrea (University of Torino) for performing the micromill sampling. We thank Emanuele Costa (University of Torino) for ICP-OES measurements, Simona Cavagna (University of Torino) for help with microprobe measurements, Andrea Festa for field assistance, and Erica Bicchi for micropalaeontological analyses. Xavi Prieto Mollar (MARUM, Bremen) helped with the measurement of compound-specific isotopes. Comments of the Editor Thierry Corrège and two anonymous reviewers improved the text. Financial support was provided by MIUR grants to P. Clari and by IAS postgraduate grant (2nd session, 2008).

References

635

636 Aloisi, G., Pierre, C., Rouchy, J.M., Foucher, J.P., Woodside, J., Party, M.S., 2000. Methane-
637 related authigenic carbonates of eastern Mediterranean Sea mud volcanoes and their possible
638 relation to gas hydrate destabilisation. Earth and Planetary Science Letters 184, 321-338.
639

640 Astin, T.R., Scotchman, I.C., 1988. The diagenetic history of some septarian concretions from the
641 Kimmeridge Clay, England. Sedimentology 35, 349-368.
642

643 Bahr, A., Pape, T., Abegg, F., Bohrmann, G., van Weering, T., Ivanov, M.K., 2010. Authigenic
644 carbonates from the eastern Black Sea as an archive for shallow gas hydrate dynamics – results
645 from the combination of CT imaging with mineralogical and stable isotope analyses. Marine and
646 Petroleum Geology 27, 1819-1829.
647

648 Baker, P.A., Kastner, M., 1981. Constraints on the formation of sedimentary dolomite. Science
649 213, 214-216.
650

651 Biddle, J.F., Lipp, J.S., Lever, M.A., Lloyd, K.G., Sørensen, K.B., Anderson, R., Fredricks, H.F.,
652 Elvert, M., Kelly, T.J., Schrag, D.P., Sogin, M.L., Brenchley, J.E., Teske, A., House, C.H., Hinrichs,
653 K.-U., 2006. Heterotrophic Archaea dominate sedimentary subsurface ecosystems off Peru.
654 Proceedings of the National Academy of Sciences of the USA 103, 3846-3851.
655

656 Bigi, G., Cosentino, D., Parotto, M., Sartori, R., Scandone, P., 1990. Structural Model of Italy:
657 Geodinamic Project: Consiglio Nazionale delle Ricerche, S.EL.CA, scale 1:500,000, sheet 1.
658

659 Birgel, D., Peckmann, J., 2008. Aerobic methanotrophy at ancient marine methane seeps: a
660 synthesis. Organic Geochemistry 39, 1659-1667.
661

662 Birgel, D., Peckmann, J., Klautzsch, S., Thiel, V., Reitner, J., 2006a. Anaerobic and aerobic

663 oxidation of methane at Late Cretaceous seeps in the Western Interior Seaway, USA.
664 Geomicrobiology Journal 23, 565-577.
665
666 Birgel, D., Thiel, V., Hinrichs, K.-U., Elvert, M., Campbell, K.A., Reitner, J., Farmer, J.D.,
667 Peckmann, J., 2006b. Lipid biomarker patterns of methane-seep microbialites from the Mesozoic
668 convergent margin of California. Organic Geochemistry 37, 1289-1302.
669
670 Birgel, D., Elvert, M., Han, X., Peckmann , J., 2008a. ^{13}C-depleted biphytanic diacids as tracers of
671 past anaerobic oxidation of methane. Organic Geochemistry 39, 152-156.
672
673 Birgel, D., Himmler, T., Freiwald, A., Peckmann, J., 2008b. A new constraint on the antiquity of
674 anaerobic oxidation of methane: Late Pennsylvanian seep limestones from southern Namibia.
675 Geology 36, 543-546.
676
677 Birgel, D., Feng, D., Roberts, H.H., Peckmann, J., 2011. Changing redox conditions at cold seeps
678 as revealed by authigenic carbonates from Alaminos Canyon, northern Gulf of Mexico. Chemical
679 Geology 285, 82-96.
680
681 Boehme, S.E., Blair, N.E., Chanton, J.P., Martens, C.S., 1996. A mass balance of ^{13}C and ^{12}C in
682 an organic-rich methane-producing marine sediment. Geochimica et Cosmochimica Acta 60, 3835-
683 3848.
684
685 Boetius, A., Ravenschlag, K., Schubert, C.J., Rickert, D., Widdel, F., Gieseke, A., Amann, R.,
686 Jørgensen, B.B., Witte, U., Pfannkuche, O., 2000. A marine microbial consortium apparently
687 mediating anaerobic oxidation of methane. Nature 407, 623-626.
688
689 Bojanowski, M.J., 2007. Oligocene cold-seep carbonates from the Carpathians and their inferred
690 relation to gas hydrates. Facies 53, 347-360.

691

692 Borowski, W.S., Paull, C.K., Ussler, W., 1999. Global and local variations of interstitial sulfate
693 gradients in deep-water, continental margin sediments: Sensitivity to underlying methane and gas
694 hydrates. Marine Geology 159, 131-154.
695
696 Budai, J.M., Martini, A.M., Walter, L.M., Ku, T.C.W., 2002. Fracture-fill calcite as a record of
697 microbial methanogenesis and fluid migration: a case study from the Devonian Antrim Shale,
698 Michigan Basin. Geofluids 2, 163-183.
699
700 Campbell, K.A., 2006. Hydrocarbon seep and hydrothermal vent paleoenvironments and
701 paleontology: Past developments and future research directions. Palaeogeography,
702 Palaeoclimatology, Palaeoecology 232, 362-407.
703
704 Clari, P., Cavagna, S., Martire, L., Hunziker, J., 2004. A Miocene mud volcano and its plumbing
705 system: A chaotic complex revisited (Monferrato, NW Italy). Journal of Sedimentary Research 74,
706 662-676.
707
708 Clari, P., Dela Pierre, F., Martire, L., Cavagna, S., 2009. The Cenozoic CH_4-derived carbonates of
709 Monferrato (NW Italy): A solid evidence of fluid circulation in the sedimentary column. Marine
710 Geology 265, 167-184.
711
712 Dahlmann, A., de Lange, G.J., 2003. Fluid-sediment interactions at Eastern Mediterranean mud
713 volcanoes: a stable isotope study from ODP Leg 160. Earth and Planetary Science Letters 212,
714 377-391.
715
716 De Boever, E., Birgel, D., Thiel, V., Muchez, P., Peckmann, J., Dimitrov, L., Swennen, R., 2009.
717 The formation of giant tubular concretions triggered by anaerobic oxidation of methane as revealed
718 by archaeal molecular fossils. Palaeogeography, Palaeoclimatology, Palaeoecology 280, 23-36.

719

720 Dela Pierre, F., Martire, L., Natalicchio, M., Clari, P.A., Petrea, C., 2010. Authigenic carbonates in
721 the upper Miocene sediments of the Tertiary Piedmont Basin (NW Italy): vestiges of an ancient gas
722 hydrate stability zone. Geological Society of America Bulletin 122, 994-1010.

723

724 DeLong, E.F., King, L.L., Massana, R., Cittone, H., Murray, A., Schlepper, C., Wakeham, S.G.,
725 1998. Dibiphytanyl ether lipids in nonthermophilic crenarchaeotes. Applied and Environmental
726 Microbiology 64, 1133-1138.

727

728 De Rosa, M., Gambacorta, A., 1988. The lipids of archaebacteria. Progress in Lipid Research 27,
729 153-175.

730

731 Elvert, M., Suess, E., Whiticar, M.J., 1999. Anaerobic methane oxidation associated with marine
732 gas hydrates: superlight C-isotopes from saturated and unsaturated C-20 and C-25 irregular
733 isoprenoids. Naturwissenschaften 86, 295-300.

734

735 Elvert, M., Boetius, A., Knittel, K., Jørgensen, B.B., 2003. Characterization of specific membrane
736 fatty acids as chemotaxonomic markers for sulfate-reducing bacteria involved in anaerobic
737 oxidation of methane. Geomicrobiology Journal 20, 403-419.

738

739 Elvert, M., Hopmans, E.C., Treude, T., Boetius, A., Suess, E., 2005. Spatial variations of
740 methanotrophic consortia at cold methane seeps: Implications from a high-resolution molecular
741 and isotopic approach. Geobiology 3, 195-209.

742

743 Fritz, P., Smith, O.G.W., 1970. The isotopic composition of secondary dolomite. Geochimica et
744 Cosmochimica Acta 34, 1161-1173.

745

746 Ghibaudo, G., Clari, P., Perello, M., 1985. Litostratigrafia, sedimentologia ed evoluzione tettonico-
747 sedimentaria dei depositi miocenici del margine sud-orientale del Bacino Terziario Ligure-
748 Piemontese (valli Borbera, Scrivia e Lemme). Bollettino della Società Geologica Italiana 104, 349-
749 397.
750
751 Gieskes J.M., Lawrence, J.R., 1981. Alteration of volcanic matter in deep sea sediments: evidence
752 from Deep Sea Drilling cores. Geochimica et Cosmochimica Acta 45, 1687.
753
754 Goossens, H., De Leeuw, J.W., Schenck, P.A., Brassell, S.C., 1984. Tocopherols as likely
755 precursors of pristane in ancient sediments and crude oils. Nature 312, 440-442.
756
757 Greinert, J., Bohrmann, G., Suess, E., 2001. Methane-venting and gas hydrate-related carbonates
758 at the Hydrate Ridge: Their classification, distribution and origin. In: Paull, C.K., Dillon, W.P.,
759 (Eds.), Natural Gas Hydrates: Occurrence, Distribution, and Detection, Geophysical Monograph
760 124, pp. 99-113.
761
762 Han, X.Q., Suess, E., Sahling, H., Wallmann, K., 2004. Fluid venting activity on the Costa Rica
763 margin: new results from authigenic carbonates. International Journal of Earth Sciences 93, 596-
764 611.
765
766 Heindel, K., Birgel, D., Peckmann, J., Kuhnert, H., Westphal, H., 2010. Formation of deglacial
767 microbialites in coral reefs off Tahiti (IODP 310) involving sulfate-reducing bacteria. Palaios 25,
768 618-635.
769
770 Hendry, J.P., Pearson, M.J., Trewin, N.H., Fallick, A.E., 2006. Jurassic septarian concretions from
771 NW Scotland record interdependent bacterial, physical and chemical processes of marine mudrock
772 diagenesis. Sedimentology 53, 537-565.
773

774 Hilgen, F.J., Krijgsman, W., Langereis, C.G., Lourens, L.J., Santarelli A., Zachariasse, W.J., 1995.
775 Extending the astronomical (polarity) time scale into the Miocene. Earth and Planetary Science
776 Letters 136, 495-510.
777
778 Himmler, T., Freiwald, A., Stollhofen, H., Peckmann, J., 2008. Late Carboniferous hydrocarbon-
779 seep carbonates from the glaciomarine Dwyka Group, southern Namibia. Palaeogeography,
780 Palaeoclimatology, Palaeoecology 257, 185-197.
781
782 Hinrichs, K.-U., Hayes, J.M., Sylva, S.P., Brewer, P.G., DeLong, E.F., 1999. Methane-consuming
783 archaebacteria in marine sediments. Nature 398, 802-805.
784
785 Hinrichs, K.-U., Summons, R.E., Orphan, V., Sylva, S.P., Hayes, J.M., 2000. Molecular and
786 isotopic analysis of anaerobic methane-oxidizing communities in marine sediments. Organic
787 Geochemistry 31, 1685-1701.
788
789 Hoffmann-Sell, L., Birgel, D., Arning, E.T., Föllmi, K.B., Peckmann, J., 2011. Archaeal lipids in
790 Neogene dolomites (Monterey and Sisquoc Formations, California) – planktic versus benthic
791 archaeal sources. Organic Geochemistry 42, 593-604.
792
793 Hounslow, M.W, 1997. Significance of localized pore pressures to the genesis of septarian
794 concretions. Sedimentology 44, 1133-1147.
795
796 Irwin, H., Cultis, C., Coleman, M., 1977. Isotopic evidence for source of diagenetic carbonates
797 formed during burial of organic-rich sediments. Nature 269, 209-213.
798
799 Iversen, N., Jørgensen, B.B., 1985. Anaerobic methane oxidation rates at the sulphate-methane
800 transition in marine sediments from Kattegat and Skagerrak (Denmark). Limnology and
801 Oceanography 30, 944-955.

802
803 Kastner, M., 1984. Sedimentology: control of dolomite formation. Nature 5985, 410–411.
804
805 Kenward, P.A., Goldstein, R.H., Gonzalez, L.A., Roberts, J.A., 2009. Precipitation of low-
806 temperature dolomite from an anaerobic microbial consortium: the role of methanogenic Archaea.
807 Geobiology 7, 556-565.
808
809 King, L.L., Pease, T.K., Wakeham, S.G., 1998. Archaea in Black Sea water column particulate
810 matter and sediments - evidence from ether lipid derivatives. Organic Geochemistry 28, 677-688.
811
812 Knittel, K., Lösekann, T., Boetius, A., Kort, R., Amann, R., 2005. Diversity and distribution of
813 methanotrophic archaea at cold seeps. Applied and Environmental Microbiology 71, 467-479.
814
815 Koga, Y., Nishihara, M., Morii, H., Akagawa-Matsushita, M., 1993. Ether lipids of methanogenic
816 bacteria: structures, comparative aspects, and biosyntheses. Microbiological Reviews 57, 164-182.
817
818 Koga, Y., Morii, H., Akagawa-Matsushita, M., Ohga, M., 1998. Correlation of polar lipid composition
819 with 16S rRNA phylogeny in methanogens. Further analysis of lipid component parts. Bioscience,
820 Biotechnology, and Biochemistry 62, 230-236.
821
822 Kuechler, R.R., Birgel, D., Kiel, S., Freiwald, A., Goedert, J.L., Thiel, V., Peckmann, J., 2011.
823 Miocene methane-derived carbonates from southwestern Washington, USA and a model for
824 silicification at seeps. Lethaia, DOI: 10.1111/j.1502-3931.2011.00280.x.
825
826 Lipp, J.S., Hinrichs, K.-U., 2009. Structural diversity and fate of intact polar lipids in marine
827 sediments. Geochimica et Cosmochimica Acta 73, 6816-6833.
828

829 Londry, K.L., Jahnke, L.L., Des Marais, D.J., 2004. Stable carbon isotope ratios of lipid biomarkers
830 of sulfate-reducing bacteria. Applied and Environmental Microbiology 70, 745-751.
831
832 Londry, K.L., Dawson, K.G., Grover, H.D., Summons, R.E., Bradley, A.S., 2008. Stable carbon
833 isotope fractionation between substrates and products of *Methanosarcina barkeri*. Organic
834 Geochemistry 2008, 608-621.
835
836 Martens, C.S., Berner, R.A., 1974. Methane production in the interstitial waters of sulfate-depleted
837 marine sediments. Science 185, 1167-1169.
838
839 Martire, L., Natalicchio, M., Petrea, C., Cavagna, S., Clari, P., Dela Pierre F., 2010. Petrographic
840 evidence of the past occurrence of gas hydrates in the Tertiary Piedmont Basin (NW Italy). Geo-
841 Marine Letters 30, 461-476.
842
843 Mazzini, A., Ivanov, M.K., Parnell, J., Stadnitskaia, A., Cronin, B.T., Poludetkina, E., Mazurenko,
844 L., van Weering, T.C.E., 2004. Methane-related authigenic carbonates from the Black Sea:
845 geochemical characterisation and relation to seeping fluids. Marine Geology 212, 153-181.
846
847 Mazzini, A., Ivanov, M.K., Nermoen, A., Bahr, A., Borhmann, G., Svensen, H., Planke, S., 2008.
848 Complex plumbing systems in the near subsurface: geometries of authigenic carbonates from
849 Dolgovskoy Mound (Black Sea) constrained by analogue experiments. Marine and Petroleum
850 Geology 25, 457-472.
851
852 Mazzullo, S.J., 2000. Organogenic dolomitization in peritidal to deep-sea sediments. Journal of
853 Sedimentary Research 70, 10-23.
854
855 McCrea, J.M., 1950. On the isotopic chemistry of carbonates and a paleotemperature scale.
856 Journal of Chemical Physics 18, 849-857.

857

858 McKenzie, J.A., Jenkyns, H.C., Bennet, G.G., 1979. Stable isotope study of the cyclic diatomite-
859 claystones from the Tripoli Formation, Sicily: a prelude to the Messinian Salinity crisis:
860 Palaeogeography, Palaeoclimatology, Palaeoecology 29, 125-141.
861
862 Meister, P., Bernasconi, S.M, Vasconcelos, C., McKenzie, J.A., 2008. Sea level changes control
863 diagenetic dolomite formation in hemipelagic sediments of the Peru Margin. Marine Geology 252,
864 166-173.
865
866 Meister, P., Gutjahr, M., Frank, M., Bernasconi, S.M., Vasconcelos, C., McKenzie, J.A., 2011.
867 Dolomite formation within the methanogenic zone induced by tectonically driven fluids in the Peru
868 accretionary prism. Geology 39, 563-566.
869
870 Mozley, P.S., Burns, S.J., 1993. Oxygen and carbon isotopic composition of marine carbonate
871 concretions: an overview. Journal of Sedimentary Petrology 63, 73-83.
872
873 Mosca, P., Polino, R., Rogledi, S., Rossi, M., 2009. New data for the kinematic interpretation of the
874 Alps–Apennines junction (Northwestern Italy). International Journal of Earth Sciences 99, 833-849.
875
876 Naehr, T.H., Birgel, D., Bohrmann, G., McDonald, I.R., Kasten, S., 2009. Biogeochemical controls
877 on authigenic carbonate formation at the Chapopote ‘‘asphalt volcano’’, Bay of Campeche.
878 Chemical Geology 266, 390-402.
879
880 Niemann, H., Elvert, M., 2008. Diagnostic lipid biomarker and stable carbon isotope signatures of
881 microbial communities mediating the anaerobic oxidation of methane with sulphate. Organic
882 Geochemistry, 39, 1668-1677.
883

884 Niemann, H., Lösekann, T., deBeer, D., Elvert, M., Nadalig, T., Knittel, K., Amann,R., Sauter, E.J.,
885 Schlüter, M., Klages, M., Foucher, J.P., Boetius, A., 2006. Novel microbial communities of the
886 Haakon Mosby mud volcano and their role as a methane sink. Nature 443, 854-858.
887
888 Nyman, S.L., Nelson, C.S., Campbell, K.A., 2010. Late Miocene analogue for the subsurface
889 plumbing of modern Hikurangi Margin cold seeps: evidence from tubular concretions in southern
890 Hawke's Bay. Marine Geology 272, 319-336.
891
892 Orphan, V.J., House, C.H., Hinrichs, K.-U., McKeegan, K.D., DeLong, E.F., 2001. Methane-
893 consuming archaea revealed by directly coupled isotopic and phylogenetic analysis. Science 293,
894 484-487.
895
896 Orphan, V.J., House, C.H., Hinrichs, K.-U., McKeegan, K.D., Delong E.F., 2002. Multiple archaeal
897 groups mediate methane oxidation in anoxic cold seep sediments. Proceedings of the National
898 Academy of Sciences USA 99, 7663-7668.
899
900 Orszag-Sperber, F., 2006. Changing perspectives in the concept of Lago-Mare" in Mediterranean
901 Late Miocene evolution. Sedimentary Geology 188–189, 259-277.
902
903 Pancost, R.D., Sinninghe Damsté, J.S., de Lint, S., van der Maarel, M.J.E.C., Gottschal, J.C.,
904 Party, Medinaut Shipboard Scientific Party, 2000. Biomarker evidence for widespread anaerobic
905 methane oxidation in Mediterranean sediments by a consortium of methanogenic archaea and
906 bacteria. Applied and Environmental Microbiology 66, 1126-1132.
907
908 Pancost, R.D., Bouloubassi, I., Aloisi, G., Sinninghe Damsté, J.S., Medinaut Shipboard Scientific
909 Party, 2001a. Three series of non-isoprenoidal dialkyl glycerol diethers in cold-seep carbonate
910 crusts. Organic Geochemistry 32, 695-707.
911

912 Pancost, R.D., Hopmans, E.C., Sinninghe Damsté, J.S., Medinaut Shipboard Scientific Party,
913 2001b. Archaeal lipids in Mediterranean cold seeps: Molecular proxies for anaerobic methane
914 oxidation. Geochimica et Cosmochimica Acta 65, 1611-1627.
915
916 Pancost, R.D., Coleman, J.M., Love, G.D., Chatzi, A., Bouloubassi, I., Snape, C.E., 2008.
917 Kerogen-bound glycerol dialkyl tetraether lipids released by hydropyrolisis of marine sediments: a
918 bias against incorporation of sedimentray organisms? Organic Geochemistry 39, 1359-1371.
919
920 Peckmann, J., Thiel, V., 2004. Carbon cycling at ancient methane-seeps. Chemical Geology 205,
921 443-467.
922
923 Peckmann, J., Thiel, V., Michaelis, W., Clari, P., Gaillard, C., Martire, L., Reitner, J., 1999. Cold
924 seep deposits of Beauvoisin (Oxfordian; southeastern France) and Marmorito (Miocene; northern
925 Italy): microbially induced authigenic carbonates. International Journal of Earth Sciences 88, 60-75.
926
927 Peckmann, J., Kiel, S., Sandy, M.R., Taylor, D.G., Goedert, J.L., 2011. Mass occurrences of the
928 brachiopod *Halorella* in Late Triassic methane-seep deposits, eastern Oregon. The Journal of
929 Geology 119, 207-220.
930
931 Pierre, C., Rouchy, J.M., 2004. Isotopic compositions of diagenetic dolomites in the Tortonian
932 marls of the Western Mediterranean margins: Evidence of past gas hydrate formation and
933 dissociation. Chemical Geology 205, 469-484.
934
935 Pierre, C., Rouchy, J.M., Blanc-Valleron, M.M., 1998. Sedimentological and stable isotope
936 changes at the Messinian-Pliocene boundary in the eastern Mediterranean (Holes 968A, 969A,
937 969B). In: Robertson, A.H.F., Emeis, K.C., Richter, C., Camerlenghi, A., (Eds.), Proceedings of the
938 Ocean Drilling Program: Scientific Results 160, pp. 3-8.
939

940 Raiswell, R., Fisher, Q.J., 2000. Carbonate concretions: a review of growth mechanisms and their
941 influence on chemical and isotopic composition. Journal of the Geological Society 157, 239-257.
942
943 Raiswell, R., Fisher, Q.J., 2004. Rates of carbonate cementation associated with sulphate
944 reduction in DSDP/ODP sediments: implications for the formation of concretions. Chemical
945 Geology 211, 71-85.
946
947 Raiswell, R.; Bottrell, S.H., McCaffrey, S.P., Marshall, J.D., McElhinney, A., Hatfield, D., 2002.
948 Isotopic constraints on growth conditions of multiphase calcite-pyrite-barite concretions in
949 Carboniferous mudstones. Sedimentology 49, 237-254.
950
951 Ritger, S., Carson, B., Suess, E., 1987. Methane-derived authigenic carbonates formed by
952 subduction-induced pore-water expulsion along the Oregon/Washington margin. Geological
953 Society of America Bulletin 98, 147-156.
954
955 Roberts, H.H., Aharon, P., 1994. Hydrocarbon-derived carbonate buildups of the northern Gulf of
956 Mexico continental slope: a review of submersible investigations. Geo-Marine Letters 14, 135-148.
957
958 Roberts, H.H., Feng, D., Joye, S.B., 2010. Cold seep carbonates of the middle and lower
959 continental slope, northern Gulf of Mexico. Deep-Sea Research II 57, 2040-2054.
960
961 Rossel, P.E., Elvert, M., Ramette, A., Boetius, A., Hinrichs, K.-U., 2011. Factors controlling the
962 distribution of anaerobic methanotrophic communities in marine environments: Evidence from
963 intact polar membrane lipids. Geochimica et Cosmochimica Acta 75, 164-184.
964
965 Rütters, H., Sass, H., Cypionka, H., Rullkötter, J., 2001. Monoalkylether phospholipids in the
966 sulfate-reducing bacteria *Desulfosarcina variabilis* and *Desulforhabdus amnigenus*. Archives of
967 Microbiology 176, 435-442.

968

969 Sample, J.C., Kopf, A., 1995. Occurrences and geochemistry of syntectonic carbonate cements
970 and veins from ODP Leg 146: implications for hydrogeologic evolution of the Cascadia margin. In:
971 Carson, B., Westbrook, G.K., Musgrave, R.J., Suess, E., (Eds.), Proceedings of the Ocean Drilling
972 Program: Scientific results 146, pp.137-150.

973

974 Schouten, S., Hopmans, E.C., Pancost, R.D., Sinninghe Damsté, J.S., 2000. Widespread
975 occurrence of structurally diverse tetraether membrane lipids: evidence for the ubiquitous presence
976 of low-temperature relatives of hyperthermophiles. Proceedings of the National Academy of
977 Sciences USA 97, 14421-14426.

978

979 Scotchman, I.C., Carr, A.D., Astin, T.R., Kelly, J., 2002. Pore fluid evolution in the Kimmeridge clay
980 formation of the UK Outer Moray Firth: implications for sandstone diagenesis. Marine and
981 Petroleum Geology 19, 247-273.

982

983 Selles-Martinez, J., 1996. Concretion morphology, classification and genesis. Earth-Science
984 Reviews 41, 177-210.

985

986 Sivan, O., Schrag, D.P., Murray, R.W., 2007. Rates of methanogenesis and methanotrophy in
987 deep-sea sediments. Geobiology 5, 141-151.

988

989 Teixidor, P., Grimalt, J.O., Pueyo, J.J., Rodriguez-Valea, F., 1993. Isopranylglycerol diethers in
990 nonalkaline evaporitic environment. Geochimica et Cosmochimica Acta 57, 4479-4490.

991

992 Thiel, V., Blumenberg, M., Pape, T., Seifert, R., Michaelis, W., 2003. Unexpected occurrence of
993 hopanoids at gas seeps in the Black Sea. Organic Geochemistry 34, 81-87.

994

995 Ussler III, W., Paull, C.K., 1995. Effects of ion exclusion and isotopic fractionation on pore water
996 geochemistry during gas hydrate formation and decomposition. Geo-Marine Letters 15, 37-44.
997
998 Ussler III, W., Paull, C.K., 2008. Rates of anaerobic oxidation of methane and authigenic carbonate
999 mineralization in methane-rich deep-sea sediments inferred from models and geochemical profiles.
1000 Earth and Planetary Science Letters 266, 271-28.
1001
1002 van Lith, Y., Warthmann, R., Vasconcelos, C., and McKenzie, J. A., 2003. Microbial fossilization in
1003 carbonate sediments: a result of the bacterial surface involvement in dolomite precipitation.
1004 Sedimentology 50, 237-245.
1005
1006 Vasconcelos, C., McKenzie, J.A., Bernasconi, S., Grujic, D., Tien, A.J., 1995. Microbial mediation
1007 as a possible mechanism for natural dolomite formation at low temperatures. Nature 377, 220-222.
1008
1009 Vasconcelos, C., McKenzie, J.A., Warthmann, R., Bernasconi, S., 2005. Calibration of the $\delta^{18}O$
1010 paleo-thermometer with dolomite formed in microbial cultures and natural environments. Geology
1011 33, 317-320.
1012
1013 Wacey, D., Wright, D.T., Boyce, A.J., 2008. A stable isotope study of microbial dolomite formation
1014 in the Coorong Region, South Australia. Chemical Geology 244, 155-174.
1015
1016 Warren, J., 2000. Dolomite: occurrence, evolution and economically important associations. Earth-
1017 Sciences Reviews 52, 1-81.
1018
1019 Whiticar, M.J., Faber, E., Schoell, M., 1986. Biogenic methane formation in marine and freshwater
1020 environments: CO_2 reduction vs. acetate fermentation — isotope evidence. Geochimica et
1021 Cosmochimica Acta 50, 693-709.
1022

1023 Whiticar, M.J., 1999. Carbon and hydrogen isotope systematics of bacterial formation and
1024 oxidation of methane. Chemical Geology 161, 291-314.
1025
1026 Wright, D.T., Oren, A., 2005. Nonphotosynthetic bacteria and the formation of carbonates and
1027 evaporites through time. Geomicrobiology Journal 22, 27-53.
1028
1029 Wright, D.T., Wacey, D., 2004. Sedimentary dolomite: a reality check. In: Braithwaite, C.J.R., Rizzi
1030 G., Darke, G., (Eds.), The Geometry and Petrogenesis of Dolomite Hydrocarbon Reservoirs,
1031 Geological Society of London, Special Pubblication 235, pp. 65-74.

FIGURE CAPTIONS

Fig. 1 Structural sketch map of northwestern Italy (modified from Bigi et al., 1990). VVL: Villalvernia Varzi Line; SVZ: Sestri Voltaggio Zone

Fig. 2 Simplified geological sketch of the studied area (modified from Ghibaudo et al., 1985) showing the location of the measured stratigraphic sections.

Fig. 3 (A) The stacking pattern of the carbonate-rich beds recognised in the upper member of SAF, reconstructed after the measurement of three stratigraphic sections. (B) Location of the studied samples in the septarian-like bed and their isotopic signature. VVC: Valle Versa chaotic complex; SAF: Sant'Agata Fossili marls

Fig. 4 (A) Outcrop view of the septarian-like bed (bed 4 in Fig.3). (B) Close-up of bed 4; note the sharp contact with the enclosing poorly consolidated sediments and the lower and upper wavy surface.

Fig. 5 (A) Polished slab of a septarian-like bed cut perpendicular to bedding, showing an intricate network of fractures filled with carbonate cements, sediments or still empty (sample DM136); the isotope signatures of the intergranular dolomite cement of both the concretion body and the clastic dykes are indicated. (B) Polished slab of the upper part of the septarian-like bed (sample ZF114) characterized by empty septarian cracks. (C-D) Photomicrographs in transmitted light (C) and in epi-fluorescence (D) of a septarian-like fracture. Note in (D) the intense autofluorescence of the dolomite-rich muddy sediments; the white arrow indicates an empty cavity. (E) Large, euhedral dolomite crystals, showing an interpenetration twinning of rhombohedral crystals. (F) Pyrite framboid composed of aggregates of hypidiomorphic cubes.

Fig. 6 (A) Unusual domal structure observed in a septarian-like bed. The lower part of the bed is affected by a major fracture system, oriented at high angle to the bedding planes; the upper part is characterized by a lobed shape and by empty septarian cracks. (B) Polished slab (sample DM115) perpendicular to bedding, revealing the high-angle fracture system, with fractures mainly filled with polyphasic carbonate cements (see Fig. 6A for location). (C) Photomicrograph showing spherulites (S) made up of different generation of carbonate cements, growing directly on the fracture walls and on clasts within the cracks.

Fig. 7 Cross-plot of the stable isotope data of carbonate phases making up the septarian-like beds and the unconsolidated marls. SAF: Sant'Agata Fossili marls.

Fig. 8 Septarian-like bed with a 5 mm wide fracture filled with polyphasic carbonate cements. The black square indicates a high-resolution transect of isotope analyses performed with the micromill technique.

Fig. 9 Synthesis of carbon and oxygen stable isotope values and biomarker results of the two types of samples analysed.

Fig. 10 Scenario showing the genesis of the septarian-like beds. See text for further details.

TABLES

Table 1 Total carbonate content and relative abundance of dolomite and calcite for the septarian-like beds and the unconsolidated marls (ICP analyses).

Table 2 Carbon and oxygen isotope composition of the septarian-like beds and of the unconsolidated marls; samples from the same fracture analysed by micromilling are marked by an asterisk (see also Fig. 7)

1090

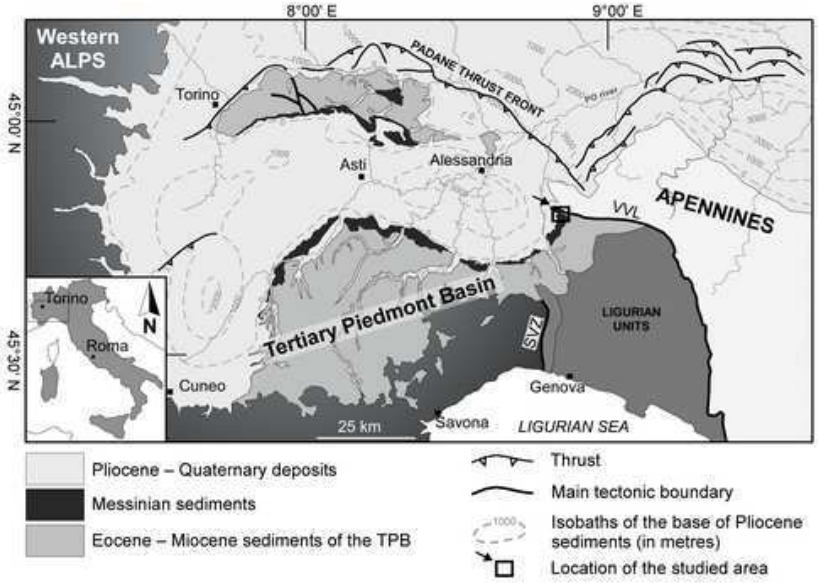

1091 Natalicchio et al. Fig.1

1092

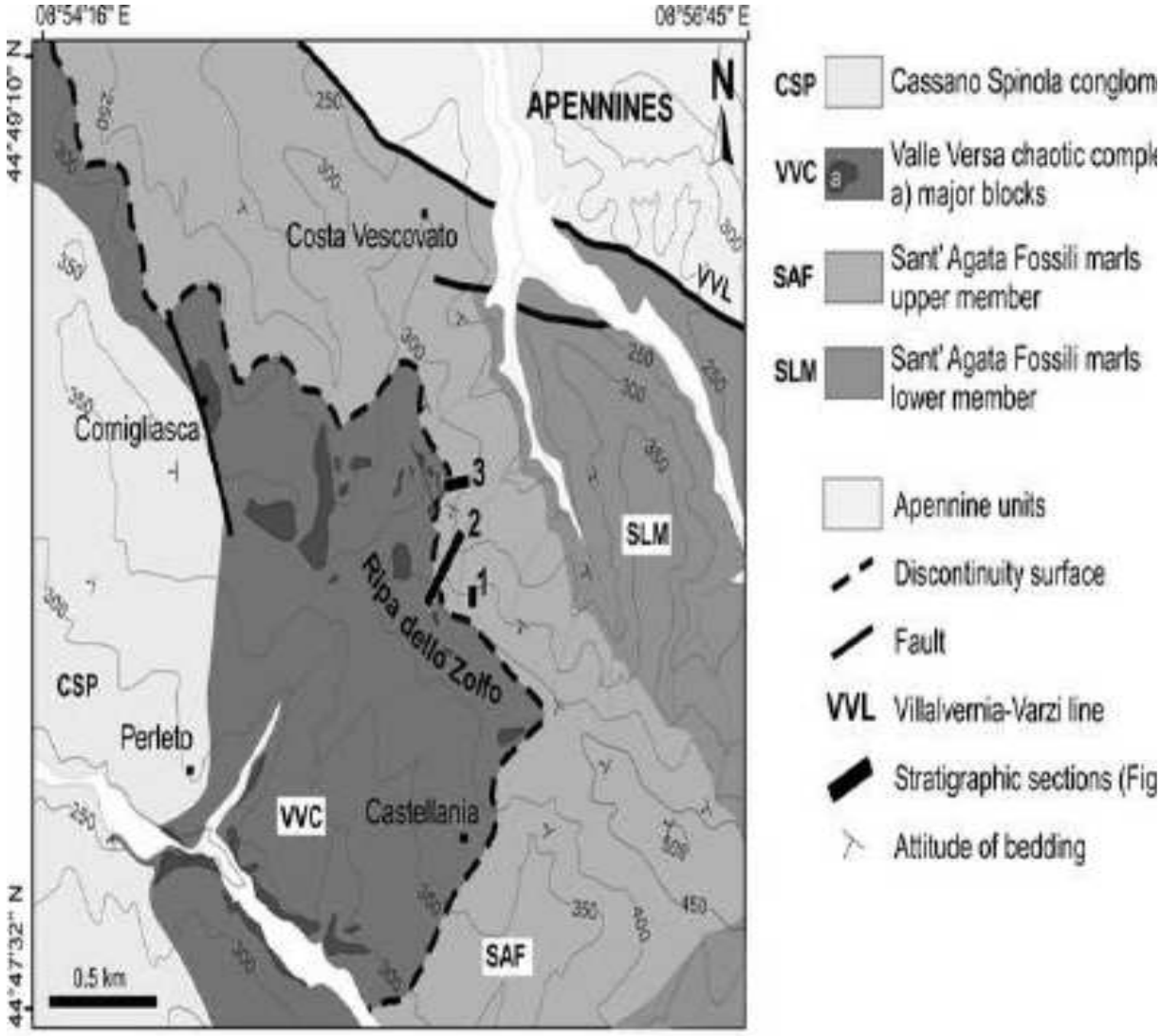

1093 Natalicchio et al. Fig.2

1094

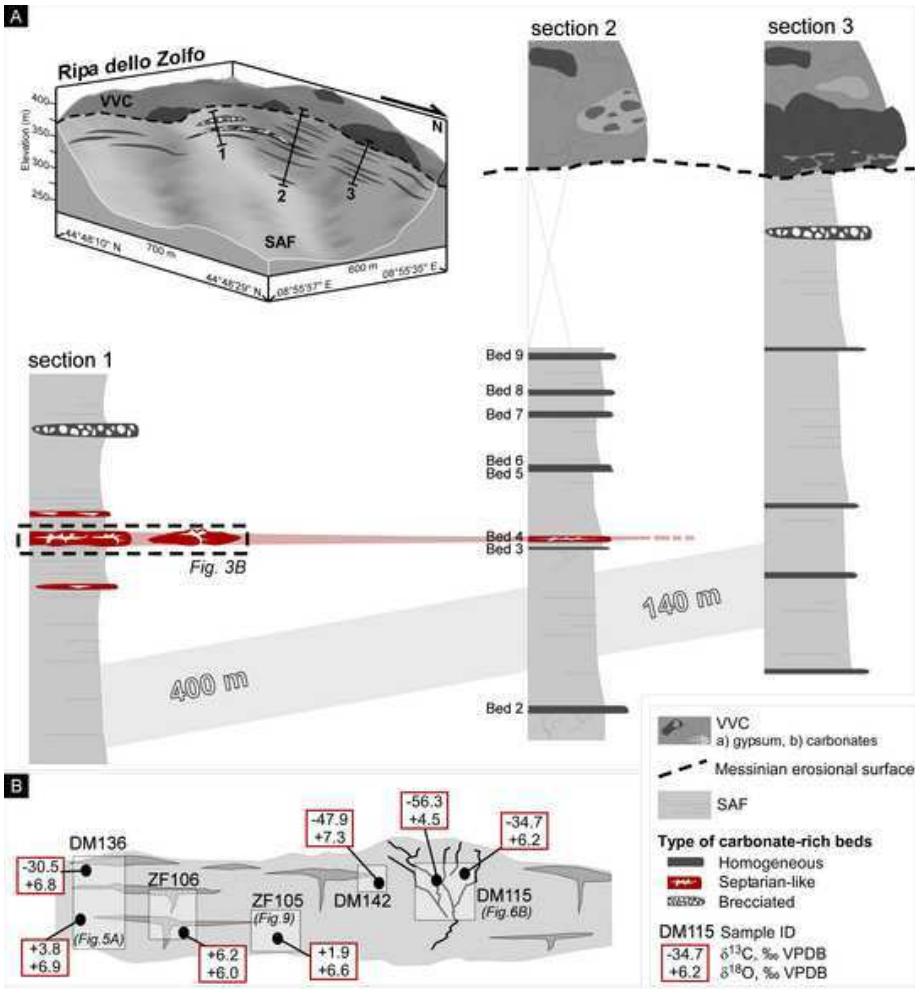

1095 Natalicchio et al. Fig.3.

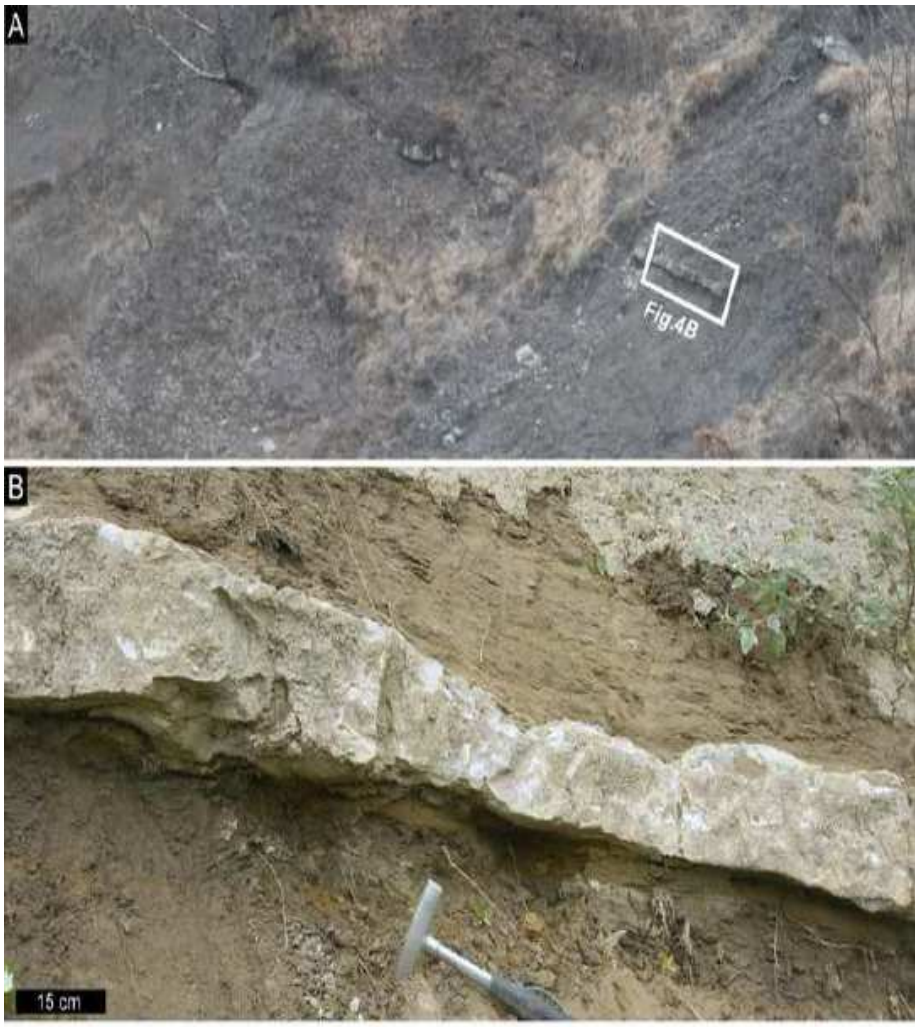

1096 Natalicchio et al. Fig.4

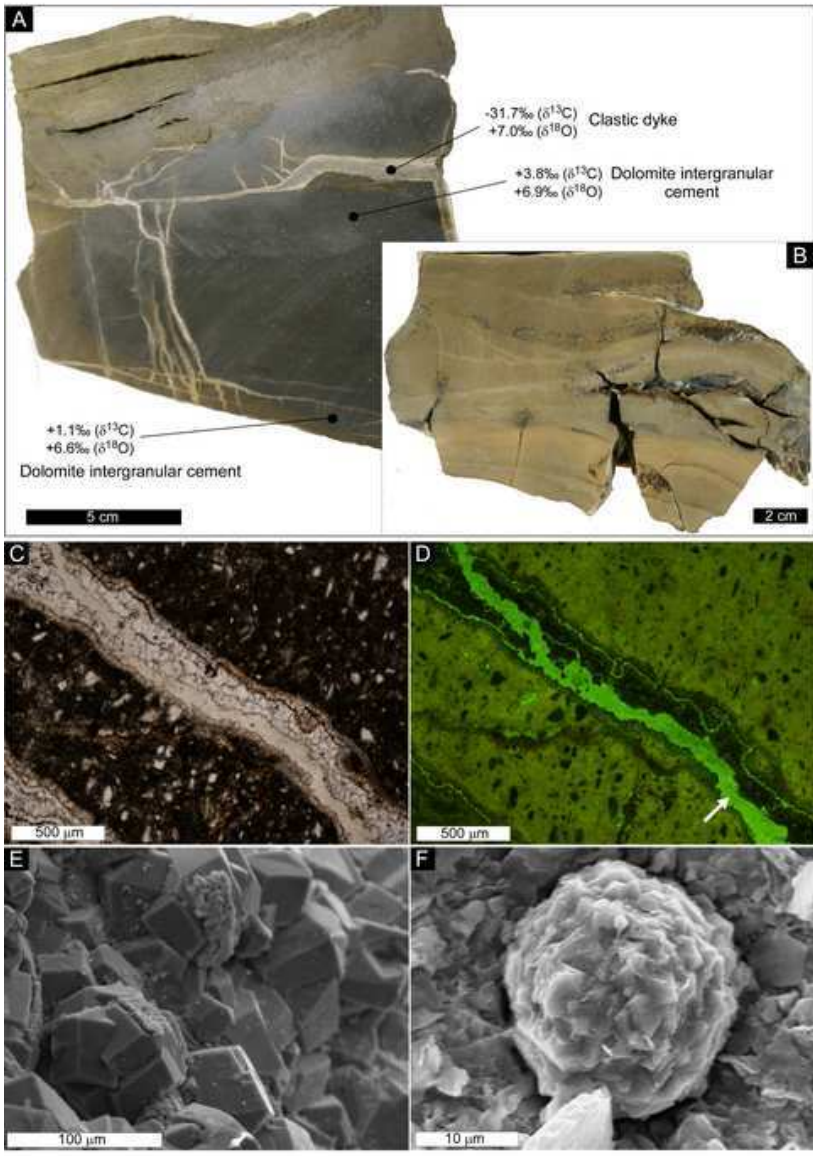

1097 Natalicchio et al. Fig.5

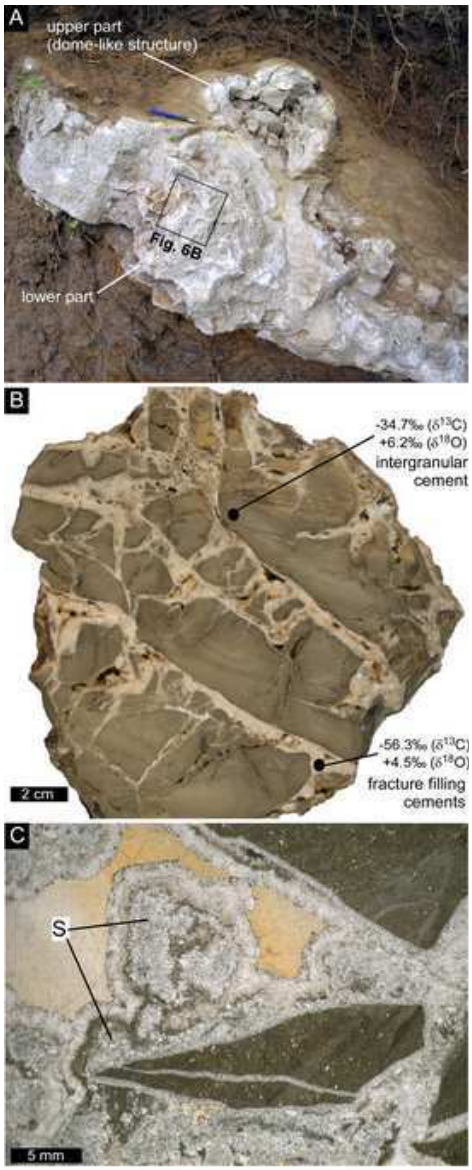

1098 Natalicchio et al. Fig.6

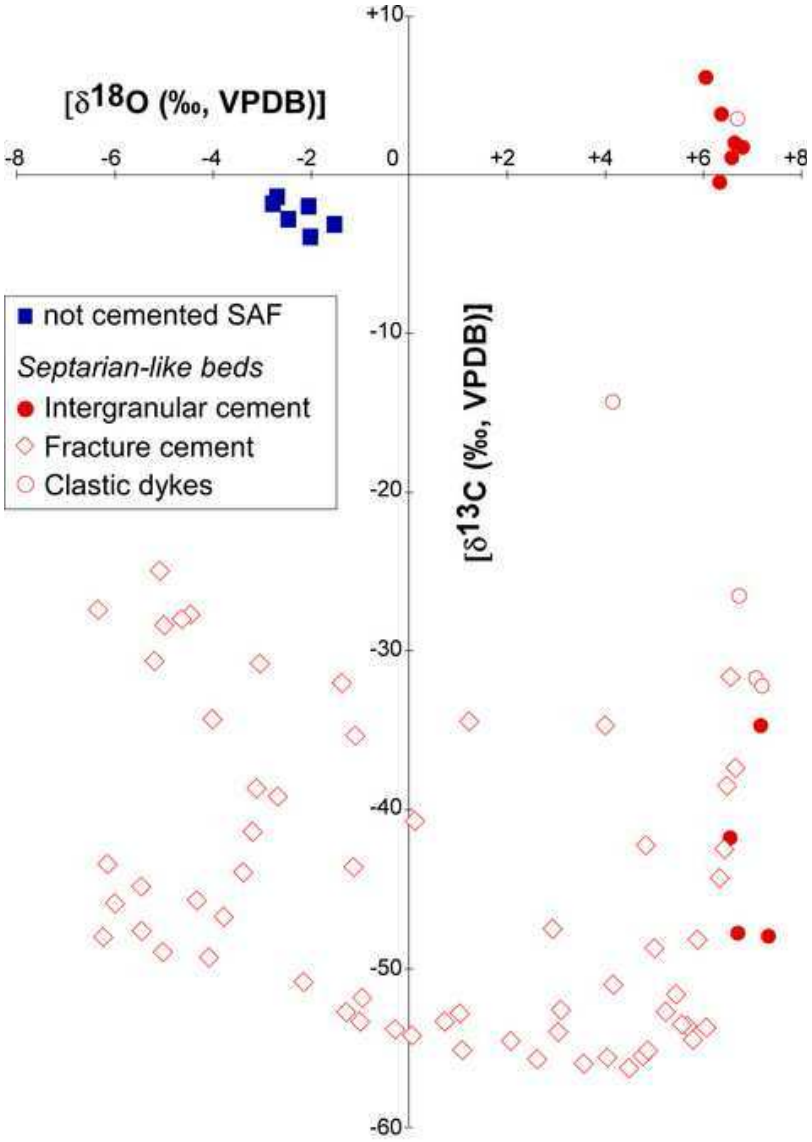

1099 Natalicchio et al. Fig.7

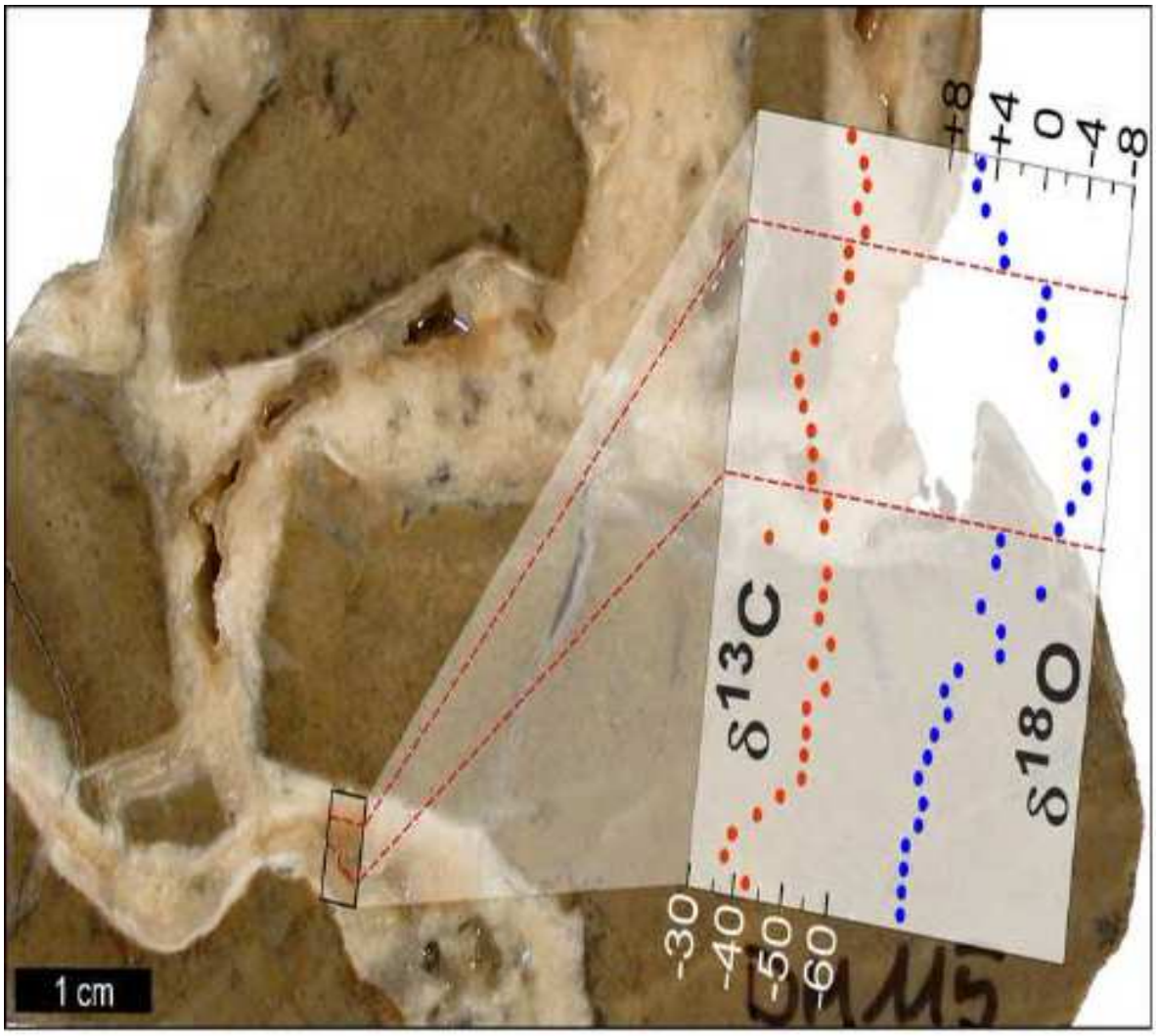

Natalicchio et al. Fig.8

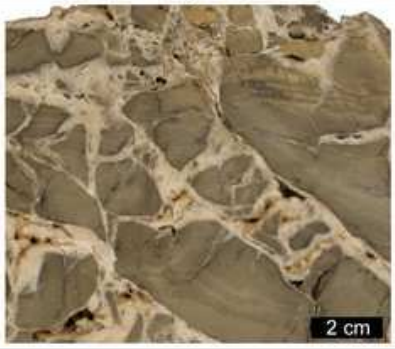

	Sample ZF105			Sample DM115		
	Type of bed: Septarian-like ***Type of analysed cement:*** intergranular			***Type of bed:*** Septarian-like ***Type of analysed cement:*** fracture filling		
	$\delta^{13}C$: 1.9‰, VPDB $\delta^{18}O$: +6.6‰, VPDB			$\delta^{13}C$: from -56.3 to -24.9‰, VPDB $\delta^{18}O$: from -6.2 to +6.5‰, VPDB		
		µg/g rock	$\delta^{13}C$ ‰ VPDB		µg/g rock	$\delta^{13}C$ ‰ VPDB
Archaeal biomarkers	phytane	tr	tr	phytane	44.0	-70
	archaeol	0.8	-40	PMI	23.3	-106
	sn-2 hydroxyarchaeol	0.4	-43	archaeol	5.4	-102
	acyclic biphytane#	57%	-22	*sn*-3 hydroxyarchaeol	13.8	-101
	monocyclic biphytane#	11%	nd	acyclic biphytanic diacid	37.4	-104
	bicyclic biphytane#	16%	nd	monocyclic biphytanic diacid	37.3	-105
	tricyclic biphytane#	16%	nd	bicyclic biphytanic diacid	17.5	-105
				acyclic biphytane#	46%	nd
				monocyclic biphytane#	33%	nd
				bicyclic biphytane#	21%	nd
Bacterial biomarkers	*iso*-$C_{15:0}$ fatty acid	0.9	nd	*iso*-$C_{15:0}$ fatty acid	2.3	nd
	anteiso-$C_{15:0}$ fatty acid	1.0	-29	*anteiso*-$C_{15:0}$ fatty acid	3.8	-75
	DAGE C_{30a}	1.5	-30	10Me$C_{16:0}$ fatty acid	10.8	-78
	DAGE C_{30b}	0.9	nd	MAGE $C_{16:0}$	4.0	-95
	DAGE C_{30c}	1.5	-30	MAGE 10Me$C_{16:0}$	2.0	nd
	17β(H),21β(H)-32-hopanoic acid	1.8	-26	17β(H),21β(H)-31-hopanoic acid	2.3	nd
				17β(H),21β(H)-32-hopanoic acid	14.8	-74
				17β(H),21β(H)-33-hopanoic acid	3.0	-74

DAGE: dialkyl glycerol ether; MAGE: monoalkyl glycerol ether; tr: traces; nd: not determined due to low contents or co-elution; #: no concentrations are available for GDGT-cleaved biphytanes, only relative proportions of the various biphytanes were calculated.

Natalicchio et al. Fig.9

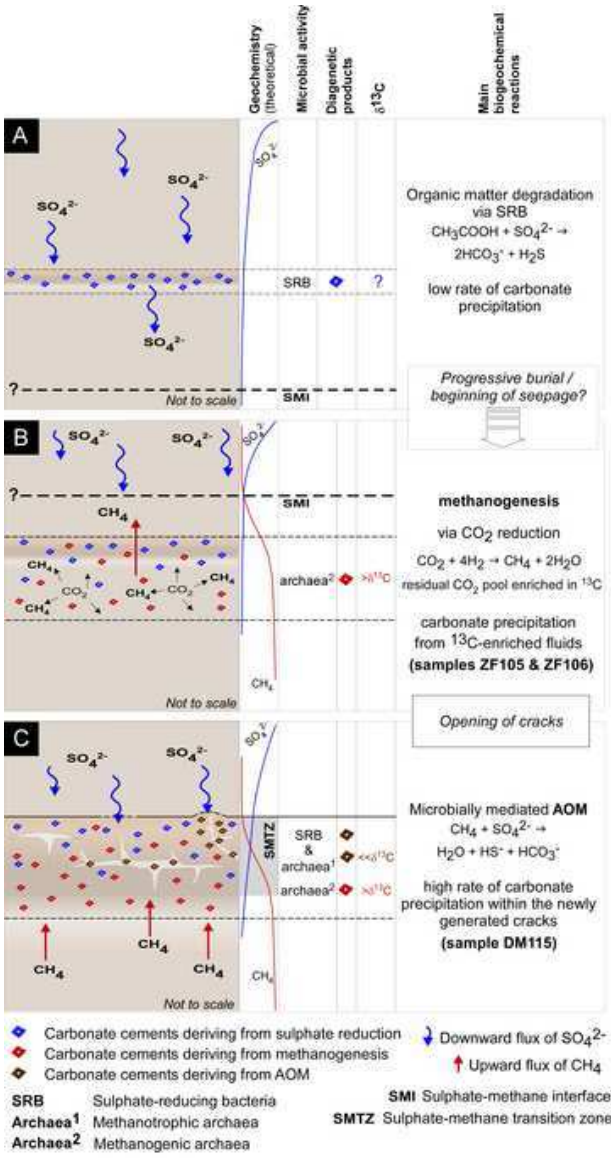

1102 Natalicchio et al. Fig.10

1103

Sample	Carbonate [wt.%]	Dolomite [%]	Calcite [%]
Septarian-like beds			
DM136T	59.5	53.5	6.0
DM136B	72.1	70.0	2.1
DM75	91.7	41.5	50.2
Marls			
OM5	13.3	5.2	8.1
OM3	15.0	5.2	9.8

1104

1105 Natalicchio et al. Tab.1

1106
1107

Sample	Cement type	$\delta^{13}C$ [‰]	$\delta^{18}O$ [‰]
Septarian-like beds			
ZF105	Intergranular cement	-0.4	+6.3
ZF105-b	Intergranular cement	+1.9	+6.6
ZF106C	Intergranular cement	+6.2	+6.0
ZF106E	Intergranular cement	+1.8	+6.8
DM115-1	Intergranular cement	-34.7	+7.2
DM136-1	Intergranular cement	+3.8	+6.4
DM136-4	Intergranular cement	+1.1	+6.6
DM142 7.3	Intergranular cement	-47.7	+6.7
DM142 7.7	Intergranular cement	-41.8	+6.5
DM142-b	Intergranular cement	-47.9	+7.3
ZF103B	carbonate vein	-34.4	+1.2
DM115-2	carbonate vein	-52.6	+3.1
DM136-5	carbonate vein	-38.7	-3.1
DM136-6	carbonate vein	-28.0	-4.6
DM137	carbonate vein	-39.2	-2.7
FM5-1	carbonate vein	-35.3	-1.1
ZF105-c	carbonate vein	-43.9	-3.4
DM142-a	carbonate vein	-30.6	-5.2
FM5-2 1.2	carbonate vein	-28.3	-5.0
FM5-2 1.3	carbonate vein	-34.7	+4.0
FM5-2 1.4	carbonate vein	-31.6	+6.5
FM5-2 1.6	carbonate vein	-30.8	-3.0
FM5-4 2.1	carbonate vein	-40.7	+0.1
FM5-4 2.2	carbonate vein	-43.6	-1.1
FM5-4 2.3	carbonate vein	-34.3	-4.0
DM115 3.1	carbonate vein	-55.2	+1.1
DM115 3.2	carbonate vein	-27.7	-4.5
DM115 3.3	carbonate vein	-55.6	+4.7
DM115 3.5	carbonate vein	-24.9	-5.1
DM 115 5	carbonate vein*	-51.6	+5.4
DM 115 6	carbonate vein*	-54.4	+5.8
DM 115 7	carbonate vein*	-55.1	+4.8
DM 115 8	carbonate vein*	-53.9	+3.0
DM 115 9	carbonate vein*	-55.7	+2.6
DM 115 10	carbonate vein*	-52.8	-1.3
DM 115 11	carbonate vein*	-53.3	-1.0
DM 115 12	carbonate vein*	-51.9	-1.0
DM 115 13	carbonate vein*	-50.8	-2.2
DM 115 14	carbonate vein*	-46.8	-3.8
DM 115 15	carbonate vein*	-43.5	-6.2
DM 115 16	carbonate vein*	-44.8	-5.5
DM 115 17	carbonate vein*	-45.8	-6.0
DM 115 18	carbonate vein*	-48.0	-6.2
DM 115 19	carbonate vein*	-49.0	-5.0
DM 115 20	carbonate vein*	-49.3	-4.1
DM 115 22	carbonate vein*	-53.3	+0.7
DM 115 23	carbonate vein*	-52.8	+1.0
DM 115 24	carbonate vein*	-41.4	-3.2
DM 115 25	carbonate vein*	-54.5	+2.0
DM 115 26	carbonate vein*	-54.1	+0.0
DM 115 27	carbonate vein*	-53.9	-0.3
DM 115 28	carbonate vein*	-56.0	+3.5
DM 115 29	carbonate vein*	-56.3	+4.5
DM 115 30	carbonate vein*	-55.6	+4.0
DM 115 31	carbonate vein*	-52.7	+5.2
DM 115 32	carbonate vein*	-53.6	+5.6
DM 115 33	carbonate vein*	-53.7	+6.0
DM 115 34	carbonate vein*	-53.5	+5.6
DM 115 36	carbonate vein*	-48.2	+5.9
DM 115 37	carbonate vein*	-44.2	+6.3
DM 115 38	carbonate vein*	-38.5	+6.5
DM 115 39	carbonate vein*	-37.4	+6.6
DM 115 40	carbonate vein*	-42.4	+6.4
DM142 7.1	carbonate vein	-48.7	+5.0
DM142 7.2	carbonate vein	-51.1	+4.2
DM142 7.4	carbonate vein	-47.6	+2.9
DM142 7.5	carbonate vein	-47.6	-5.4
DM142 7.6	carbonate vein	-45.7	-4.3
DM142 7.8	carbonate vein	-32.0	-1.3
DM142 7.9	carbonate vein	-27.4	-6.3

DM142 7.10	carbonate vein	-42.2	+4.8
DM111-2	clastic dikes	-14.3	+4.1
ZF103A	clastic dikes	-26.6	+6.7
DM136-2	clastic dikes	-31.7	+7.0
ZF106A	clastic dikes	+3.5	+6.7
ZF106B	clastic dikes	-32.2	+7.2
Marls			
DM133	Marly host-rock	-4.1	-2.1
DM134	Marly host-rock	-1.7	-3.0
DM135	Marly host-rock	-1.1	-2.8
OM1	Marly host-rock	-2.8	-1.5
OM3	Marly host-rock	-2.1	-2.0
OM9	Marly host-rock	-3.0	-2.5

Natalicchio et al., Tab.2